FACULDADE DE ENGENHARIA DA UNIVERSIDADE DO PORTO

FEUP

Reclassification of a shielding design project for facilities administering ^{131}I for thyroid carcinoma therapy

Daniela M. Guimarães

Mestrado Integrado em Bioengenharia

Supervisor: Maria do Carmo Baptista

Co-Supervisor: António Silva

31 July 2014

Resumo

O cancro da tiroide é tipo de neoplasia endócrina mais frequente, estando na maioria das vezes associado a um excelente prognóstico que deve à terapia com iodo radioativo.

Como a única função do iodo no organismo humano está relacionada com a síntese de hormonas tiroideias que ocorre na própria glândula tiroideia, este radionuclídeo apresenta uma elevada especificidade para a glândula em questão. Além disto, 80% dos casos são do tipo papilar, que possuem a capacidade de reter as funções biológicas básicas características do tecido glandular normal, como por exemplo, a capacidade de captar iodo da circulação sanguínea.

Apesar da eficácia do tratamento, grandes quantidades de energia são emitidas durante o decaimento do iodo radioativo (^{131}I), sob a forma de partículas e radiação eletromagnética, que possuem diferentes capacidades ionizantes e de penetração. Desta forma, a terapia com iodo radioativo está sujeita a regras estabelecidas pela legislação nacional, que visam minimizar a exposição à radiação dos pacientes, familiares, membros do público e trabalhadores do serviço.

Muito resumidamente, os fatores de segurança dependem do tempo de exposição, da distância à fonte radioativa e da blindagem. O objetivo deste trabalho é caracterizar e reprojetar um plano de barreiras de um quarto já existente, de forma a torná-lo apto para a administração desta terapia, tendo em conta os fatores de segurança supramencionados.

Abstract

Thyroid carcinoma is the most frequent endocrine malignancy worldwide. The excellent prognosis in an overwhelming number of cases is related to radioiodine therapy.

As the only function of iodine in the human body is the synthesis of thyroid hormones, within the thyroid gland, this radionuclide presents high specificity for this gland. Moreover, 80% of the incident cancers are papillary thyroid cancer (PTC) type, meaning that basic biologic characteristics of thyroid normal tissue are retained, such as iodine uptake from the circulating blood.

Despite the efficacy of the referred treatment, large amounts of energy are emitted during radioiodine (^{131}I) decay, in the form of particles and electromagnetic radiation with distinct ionising and penetrating powers. Therefore, the administration of ^{131}I within a nuclear medicine service must follow strict rules determined by national legislation, in order to minimise the exposure to radiation of patients, families, members of the public and workers of the facilities.

Briefly, the safety factors are related to the exposure time, distance to the radiation source and the shielding barriers. The aim of this project is therefore to characterise and redesign a shielding plan of a unit designated for the administration of ^{131}I, taking in consideration these safety factors.

Contents

List of Figures

List of Tables

List of Roman Letter Symbols

A

A activity

B

B build-up factor
Bq Becquerel (SI unit of activity)

C

c speed of light in vacuum (3×10^8 m s^{-1})
C coulomb (unit of electric charge)
Ci Curie (unit of activity: $3,7 \times 10^{10}$ s^{-1})

D

d day (unit of time)
D absorbed dose (Gy)
D distance

E

E energy
E_B binding energy
E_D effective dose (Sv)
E_K kinetic energy
eV electron volt (unit of energy: $1,6 \times 10^{-19}$ J)

G

g gram (unit of mass: 10^{-3} kg)

Gy gray (SI unit of kerma and dose: 1 J kg^{-1})

H

h hour (unit of time)
h Planck's constant ($6,626 \times 10^{-34}$ J s)
H_T equivalent dose (Sv)

I

I intensity

J

J Joule (SI unit of energy)

K

K kerma
kg kilogram (SI unit of mass)

M

m meter (SI unit of distance)
m mass

N

N Number of neutrons

P

p momentum

S

s second (unit of time)
Sv sievert (unit of equivalent dose)

T

t time

$t_{1/2}$ half-life
T_b biological half-life
T_e effective half-life

W

w_R radiation weighing factor
w_T tissue weighing factor

X

x thickness
X exposure (C kg^{-1})

Y

Y yield

Z

z height
Z number of protons; atomic number

List of Greek Letter Symbols

β

β^+ beta plus particle (positron)
β^- beta minus particle (electron)

γ

γ photon originating in a nuclear transition
Γ Exposure Rate Constant

δ

δ minimum cut-off energy

θ

θ scattering angle

κ

κ linear attenuation coefficient for pair production

λ

λ wavelength; decay constant

μ

μ linear attenuation coefficient
μ_m mass attenuation coefficient

ν

ν frequency

ρ

ρ density

σ

σ_C linear attenuation coefficient for Compton scattering
σ_R linear attenuation coefficient for Rayleigh scattering

τ

τ linear attenuation coefficient for photoelectric effect

ϕ

ϕ fluence rate
Φ fluence

List of Abbreviations

ALARA	As Low As Reasonably Achievable
ATC	Anaplastic Thyroid Cancer
DIT (or T2)	Diiodotyrosine
DTC	Differentiated Thyroid Cancer
ERC	Exposure Rate Constant
EURATOM	The European Atomic Energy Community
FTC	Follicular Thyroid Cancer
HCC	Hürthle Cell Cancer
HPT	Hypothalamic-Pituitary-Thyroid
HVL	Half-Value Layer
IR	Ionising Radiation
LET	Linear Energy Transfer
LT4	Levothyroxine
MIT (or T1)	Monoiodotyrosine
MTC	Medullary Thyroid Cancer
NIR	Non-ionising Radiation
NIS	Sodium/Iodide Symporter
OJEU	Official Journal of the European Union
PTC	Papillary Thyroid Cancer
RAI	Radioactive Iodine
rhTSH	Recombinant Human TSH
RRA	Thyroid Remnant Ablation
T3	Triiodothyronine
T4	Thyroxine or Tetraiodothyronine
TBG	Thyroxine-Binding Globulin
Tg	Thyroglobulin
TRH	Thyrotropin-Releasing Hormone
TSH	Thyroid-Stimulating Hormone
TVL	Tenth-Value Layer
UICC	Union Internationale Contre le Cancer

Chapter 1

Introduction

The only function of iodine in the human body is related to the synthesis of thyroid hormones that occurs within the thyroid tissue. As the chemical properties of radioiodine (^{131}I) are similar to the stable iodine's properties [1], thyroid cells, normal or carcinogenic, cannot distinguish between the unstable and the stable form of iodine. Therefore, this radioisotope presents high specificity to this gland and for this reason thyroid carcinoma treatment with radioactive iodine (RAI) is highly effective and popular nowadays.

Following ^{131}I decay both β-particles and γ-rays are emitted. The first represent the highest contribution to the success of the treatment, however the majority of the second ones, leave the patient via the skin surface. As a result, the patient becomes a source of radiation, which definition and undesirable consequences are explained below.

Radioactivity or radioactive decay refers to the stabilisation process of a parent nucleus into a more stable daughter nucleus accompanied by energy emission [2]. This energy is called radiation.

An atomic nucleus is characterised by the number of protons (or atomic number, Z) and by the number of neutrons (N) [2], the sum of which gives the atomic mass number. When there is no optimal equilibrium between protons and neutrons, the nucleus is said to be unstable or radioactive. When a radioactive substance contains atoms of same structure it is often referred to as radioactive nuclide. These radioactive species decay until a more stable configuration is achieved. Sometimes, this configuration is still unstable, resulting in a decay chain as far as a stable nuclide is formed [3]. The decay rate or activity (A) of a radioactive nucleus represents the total number of decays (or disintegrations) per unit time, therefore it may be expressed as

$$A = \frac{dN}{dT}, \tag{1.1}$$

where dN is the expected number of nuclear transitions from a particular energy state in a certain time interval dT. The SI unit of activity is the Becquerel (Bq), given as 1 Bq = 1 s^{-1} (one Becquerel is equivalent to one nuclear transition per second) [4].

The activity of a radioactive substance at a certain time (t) is given by an exponential law,

known as the fundamental decay equation or decay law:

$$A(t) = A(0)e^{-\lambda t}, \tag{1.2}$$

where $A(0)$ represents the initial activity (at time $t = 0$) and λ corresponds to the radioactive decay constant, a characteristic parameter for each radioactive decay process. This is the most important defining characteristic of radioactive nuclides [3]. The time at which the number of radioactive nuclei of the substance has already decayed to half of the initial value (given by dN in Equation 1.1) is called half-life, ($t_{1/2}$). The relationship between this quantity and the decay constant, λ, is given by the following equation:

$$\lambda = \frac{\ln 2}{t_{1/2}}. \tag{1.3}$$

The spontaneous radioactive decay processes are divided into three main categories. Each process is accompanied by emission of energetic particles, as can be seen in Table 1.1. The type of radioactive decay depends upon the nuclide involved.

Table 1.1: Particles emitted in the different natural radioactive decay processes (adapted from [3]).

Radioactive decay process		Particle emitted
α decay		α particles
β decay	β^-	Electrons, antineutrinos
	β^+	Positrons, neutrinos
	Electron capture	Neutrinos
γ decay	γ decay	γ rays (photons)
	Internal conversion	Atomic orbital electrons

Therefore, the decay energy is emitted either as electromagnetic radiation or in the particulate form, by particles. Nevertheless, both present wave-particle duality, meaning that they can be characterised as waves, by its amplitude, wavelength (λ) and momentum (p) that are related according to

$$\lambda = \frac{h}{p}, \tag{1.4}$$

where h is the Planck's constant (h = 6,626 $\times$ 10 $^{-34}$J s). A quantum of electromagnetic radiation is called a photon, which carries energy given by $h\nu$, where ν is the frequency given by $v = c/\lambda$, where c is the speed of light in vacuum ($c \approx 3 \times 10^8$ m s^{-1}). The energy per photon is expressed in electron volts (eV).

The ^{131}I decays by β^- emission to excited states of the daughter nuclei ^{131}Xe which decay to the fundamental state by several γ emissions (as shown in the decay scheme in Appendix A, Figure A.1). The first occurs when a nucleus has an excess of neutrons and attempts to reach

stability by converting a neutron into a proton with the emission of an electron [2]. This often results in an excited daughter nucleus that instantaneously (within 10^{-12} s) continues the decay process to its ground state emitting the excitation energy in the form of gamma ray photons [3].

When an incident beam strikes a target, its particles can interact with the target nuclei and orbital electrons by scattering, absorption and nuclear reaction. When crossing matter, the beam is attenuated in intensity (I), energy (E) or both [3]. Hereupon, radiation can be classified, as shown in Figure 1.1, as non-ionising radiation (NIR) and ionising radiation (IR). NIR cannot ionise matter because its energy is not enough to disrupt chemical bonds and remove an electron from an atom [2], while IR carries sufficient energy to remove bounds from atomic shells, thus producing ionised atoms and molecules [2]. Therefore, one can say that IR energy exceeds the ionisation potential of matter [3]. This threshold energy depends on the matter's characteristics [2].

IR can ionise matter directly or indirectly. Directly ionising radiation consists of charged particles that through direct Coulomb interaction deposit energy in the medium. In its turn, indirectly ionising radiation comprises neutral particles that deposit energy in the medium by release of a charged particle which interacts with the medium as directly IR [3].

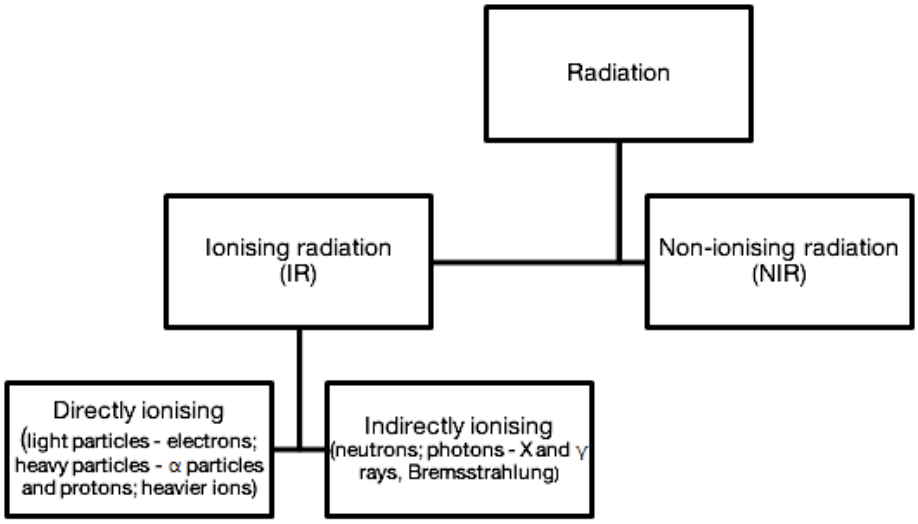

Figure 1.1: Classification of radiation (adapted from [3]).

In addition to the ionising ability, radiation is also able to penetrate through matter. The penetrating power is inversely proportional to the ionising power, since radiation continues to penetrate matter until it has lost all of its energy. Briefly, β particles have lower penetrating power than γ rays, but higher ionising power. The reason is because β particles are charged, while γ rays are electrically neutral and massless presenting relatively little interaction with matter. While for beta particles the ionisation is more localised, for gamma radiation it is more spread out, since they are not slowed by collisions.

The penetrating power of radiation is reflected in the distance that they can travel through air. β particles have a range in air of a few meters, while γ radiation can travel many meters, due to little absorption or scattering as they pass through air [5].

Both directly and indirectly IR are used for disease's diagnosis and treatment, in a branch of medicine called nuclear medicine. Thus, radioactive isotopes are injected or ingested by the patient, and it is expected that calculated doses of ionising radiation emitted during decay of these pharmaceuticals interact with metabolic or physiologic paths of the organism originating informative images or treating the disease, most often cancerous tumours. Concerning therapy purposes, radiopharmaceuticals are designed to locate with high specificity the cancerous foci, even when the location is unknown or it has already metastasised, while minimally damaging normal tissue. This behaviour depends on the chemical and physical characteristics of the isotope.

Hereupon, the radiation emitted by radioiodine that is necessary for the success of the treatment may also present a great extent of harm to all the other people around the patient. For this reason, during the radioactive treatment, the patient should be isolated within a designated unit that should follow radiation safety principles so that in the vicinity of this premises the radiation exposure values are below those established by national legislation. These measures aim to provide safety for other patients, families, members of the public and workers of the facilities.

1.1 Goals

The present work intended to redesign a shielding project for a specific room from Hospital CUF Porto's inpatient unit. The project was developed in strict collaboration with specialists from the Medical Physics Department of Dr. Campos Costa. Both entities belong to the same group, José de Mello Saúde.

The aforementioned unit was first conceived to accommodate an iodine therapy room, in particular, the highly effective thyroid carcinoma treatment, which consists in the ingestion of a specific dose of radioiodine by a patient, previously submitted to a thyroid gland removal surgery. However, proper license was not provided and the room continued to be occupied with non-radioactive treatments' patients. Currently, the Hospital CUF Porto's board is dedicated to provide this treatment to the community and, for this reason the room's characteristics should be properly reassessed in order to fulfil all the radioprotection requirements.

In order to propose an efficient shielding design for the facility in question, the work planning was essentially divided in three parts:

1. Assessment of the radiation sources properties;
2. Exhaustive characterisation of the existing unit construction materials;
3. Determination of the exact characteristics of the necessary reinforcement to effectively attenuate the radiation emitted during decay of the administered ^{131}I radiopharmaceutical to values accepted by Portuguese and European legislation.

1.2 Report Layout

This thesis is organised in seven chapters.

Chapter 1 presents a few introductory concepts necessary to the comprehension of the scope of this project. Motivation and goals of the present work are highlighted in this section, as well.

Chapter 2 presents detailed information concerning: the thyroid gland and the thyroid carcinoma (Section 2.1), where physiologic aspects concerning iodine uptake in healthy and cancerous thyroid tissue are pointed out; the ^{131}I and the therapy with the radioisotope (Section 2.2), explained how the radiation emitted during radioiodine decay destroys malignant thyroid cells. This chapter gives an insight relatively to the biomedical context of this radiotherapy and the reason for its efficiency and popularity and why there is a need for a reliable shielding plan concerning the energies and radiations involved.

Chapter 3 explains the processes by how radiation interacts with matter (Section 3.1), the biological tissue and the resulting biological effects (Section 3.3); how to characterise a radiation field (Section 3.2); how to minimise radiation exposure values towards the regulatory recommendations of radioprotection (Section 3.5 and 3.4); and how to efficiently shield a unit in a nuclear medicine service where a patient submitted to ^{131}I therapy will be isolated (Section 3.6). This chapter helps to understand the need identified in the second chapter.

Chapter 4 presents the first part of the work performed which consists in the assessment of the used radiation source properties that support the posterior experiments.

Chapter 5 characterises the unit structure materials, in the presence of different radioactive sources with different range of energy emission.

Chapter 6 proposes a shielding plan as the solution to the identified problem.

Chapter 7 shows the conclusions and possible future work developments concerning shield-optimisation aspects.

Chapter 2

Biomedical Insight

2.1 Thyroid and Thyroid Carcinoma

Thyroid carcinoma is the most frequent endocrine malignancy worldwide, present in 5% of all detected thyroid nodules, which occur annually in 20–50% of the general population [6]. The age group peak incidence is 65–69 years in men and 45–49 years in women.

In Europe, there were 3,4 million new cases of cancer in 2012, but only 52 937 of which corresponded to thyroid cancer type. Just 6 334 cases were related to death, which can be translated in a mortality of 12% concerning incidence of thyroid cancer, and of 0,2% concerning total cancer incidence. In women, thyroid cancer incidence was higher (40 654 versus 12 283 new cases in men) [7]. In Portugal, the same trend was verified. In the same year, it was registered 576 new cases (449 in women and 127 in men), associated with a mortality of 16% [8]. Hereupon, the rarity of this malignancy, along with its excellent prognosis in an overwhelming number of cases, are two of the main features of thyroid carcinoma [9].

As implied from the aforementioned statistical data, thyroid carcinoma is actually one of the most common cancer in women [8], but despite the global higher incidence, there is no generally accepted reason that may explain this sexual disparity. Thyroid cancer incidence also varies with geographic area and ethnicity, which might be justified by genetic factors, environmental influences and access to medical care [10].

As it has been observed in recent decades, increasing incidence of thyroid carcinoma is expected [11, 12, 10], as shown in Figure 2.1. This increase may be due to the more sensitive diagnostic procedures that allow the detection of small cancers in the preclinical stage. However, a true increase is also plausible, as a consequence of increased population exposure to radiation, environmental carcinogens due to the industrialised lifestyle and other still unrecognised carcinogens [10].

These considerations dictate the need for applying the more effective, less invasive and less expensive approach able to guarantee the best quality of life for a disease that requires a follow-up care throughout life, despite the intrinsic low mortality.

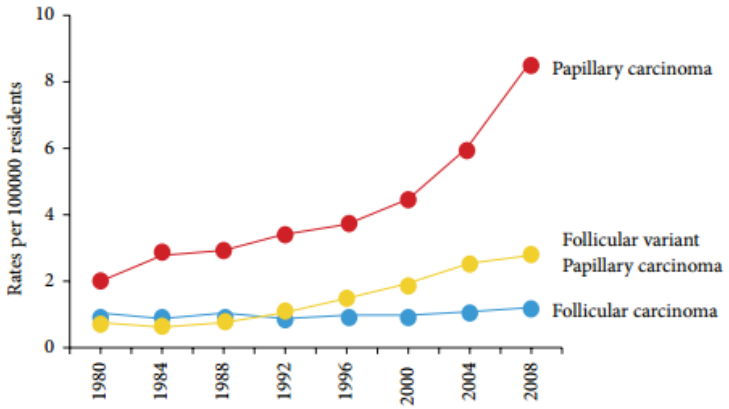

Figure 2.1: Trend in thyroid cancer incidence in the North American population from 1980 to 2008 by histotype (adapted from [11]).

2.1.1 The Thyroid Gland

The thyroid gland is the largest endocrine gland, weighing about 15–20 grams in the normal adult [13, 14].

It synthesises, stores and secretes two major hormones, required for the normal function of a variety of physiologic processes affecting nearly every organ system in the body, as metabolism, heart rate, body temperature and tissue growth. Thyroid hormones are essential for normal growth and development and are most obvious during infancy and early childhood [15].

The thyroid gland acts as an important store of iodine in the human body, from which synthesis of triiodothyronine (or T3, indicating 3 iodine atoms) and thyroxine or tetraiodothyronine (or T4, indicating 4 iodine atoms) depend. The former is more abundant, but T3 is the most potent, constituting 90% and 10% of thyroid secretion, respectively [14]. Hormone secretion is regulated by the hypothalamic-pituitary-thyroid (HPT) system [13].

Thyroid dysfunction ranges from the overproduction or underproduction of thyroid hormones, to the development of neoplasia. The possible diseases include hyperthyroidism, hypothyroidism, Grave's disease, Hashimoto's thyroiditis, goiter, adenoma (benign growths of the thyroid) and thyroid carcinoma.

2.1.1.1 Anatomy

The thyroid gland is located in the neck, inferior to the larynx and cricoid cartilage. It is formed by two lobes, each about 5 centimetres long that are joined anteriorly by a narrow isthmus, over the second and third tracheal cartilages. The lobes lay either side of the trachea and the oesophagus [16]. In the posterior region of each lobe, four parathyroid glands are located. These are responsible for the production of the parathyroid hormone [16].

The thyroid gland is surrounded by a fibrous capsule that firmly connects the thyroid gland to the larynx. This explains why the thyroid moves on swallowing. A schematic representation of the thyroid gland anatomic position might be seen in Figure 2.2.

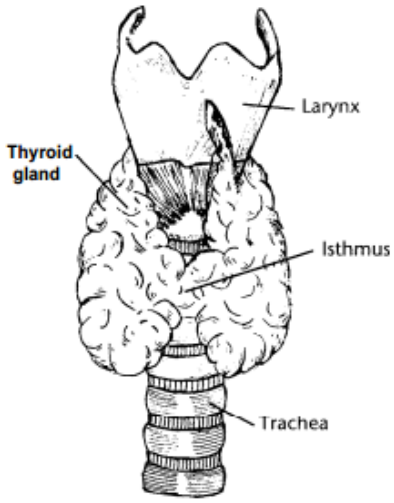

Figure 2.2: The thyroid gland (adapted from [14]).

The lobes contain about one million spherical structures called follicles, which represent the functional units of the thyroid gland (Figure 2.3). Each follicle is lined by a single layer of cells (secretory epithelial cells) around a colloid filled space. The follicular cells secrete the thyroglobulin (Tg) glycoprotein into the lumen of the follicle. Thyroid hormones are synthesised at the cell-colloid and must be bound up as residues of the Tg molecule during synthesis in order to restrict their movements, due to their lipophilicity. In this sense, Tg in the colloid acts as precursor and storage form of T3 and T4. When thyroid is actively secreting hormones, the colloid store shrinks[14].

In between follicles, parafollicular cells (C cells) are also found. These are responsible for the synthesis and secretion of calcitonin, involved in calcium homeostasis.

The thyroid is highly vascular, and consequently its appearance is more reddish than the nearby tissue [14]. It is supplied about 5 millilitres of blood per gram of thyroid tissue, by three main arteries (superior thyroid artery, inferior thyroid artery and thyroidea ima artery in just 10% of people.) [16, 15]. It is drain by three veins (superior thyroid vein, middle thyroid vein and inferior thyroid vein). The first two veins drain into the internal jugular, whereas the inferior vein drains into the brachiocephalic veins.

2.1.1.2 Hormone Synthesis and Secretion

As a part of the endocrine system, thyroid main function is to regulate hormones in the body, but unlike other endocrine glands, which secrete their hormones the moment they are produced,

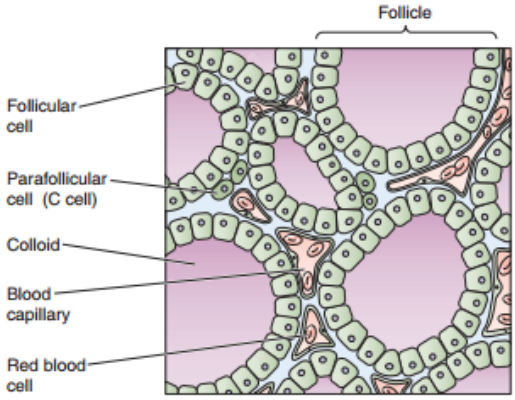

Figure 2.3: Follicular structure of the thyroid gland (adapted from [17]).

the thyroid gland stores considerable amounts of the thyroid hormones (T3 and T4) until they are needed by the body.

Thyroid hormone synthesis is a step-by-step complex process that takes place in both colloid and follicular cells. It depends on the presence of both tyrosine and iodine. Tyrosine, a non-essential aminoacid, is the major substrate that combines with iodine to form thyroid hormones. Tyrosine is converted in the interior of follicular cells into Tg glycoprotein, which contains approximately 110 tyrosine residues, in a process called *Thyroglobulin synthesis*. Unlike tyrosine, iodine concentration in the plasma is very low, so it must be provided to the body. The primarily supply is through diet (mostly dairy products and cereals), although it might be also absorbed from the skin and lungs. Seawater is also a major source of iodine, that is the reason why coastal zones tend to be the most iodine-enriched environments [18]. About 150 milligram of iodine is needed per day [18] in order to prevent irregularities, but only a fraction of this is actually absorbed by the thyroid gland cells. These are the only cells that can actively absorb plasma iodine and utilise it in the synthesis of thyroid hormones. In fact, the only role of iodine in the body is related to the synthesis of thyroid hormones and this is the main reason why the treatment of thyroid carcinoma with radioiodine is highly thyroid tissue specific, and consequently, efficient.

The initial step in the formation of thyroid hormones is the absorption and concentration of the iodide anion (I^-). Normally, 30% of iodine uptake is translocated to the thyroid and 70% directly excreted in the urine [15, 19]. In a process called *iodine trapping*, the thyroid follicle actively pumps plasma iodide ions, through the specialised Na/I cotransporter (NIS), against a concentration gradient from the extracellular fluid to the interior of the follicular cell, where it is oxidised into iodine (I) by iodide peroxidase enzyme [17]. This increases the iodine concentration in the thyroid gland by 30 times its concentration in the blood. During active stimulation, the concentration of iodine can be as high as 250 times.

Once formed, iodine rapidly attaches to tyrosine molecules within Tg (*Iodination of thyroglobulin* or *Organification of iodide*), resulting in monoiodotyrosine (MIT or T1) and diiodotyrosine

(DIT or T2). Then, in a process called *coupling*, iodotyrosines are coupled together to form iodothyronines. Two DIT molecules are coupled to form T4 (Figure 2.4) and one DIT and one MIT are joined to form T3 (Figure 2.5). Only 20% of iodinated tyrosine undergoes coupling, with the rest remaining as MIT and DIT.

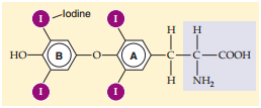

Figure 2.4: Molecular structure of thyroid hormone T4 (3,5,3',5'-tetraiodo-L-thyronine) (adapted from [17]).

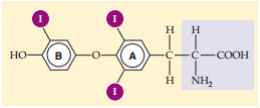

Figure 2.5: Molecular structure of thyroid hormone T3 (3,5,3'-triiodo-L-thyronine) (adapted from [17]).

At this point, thyroid hormones are stored in the follicles until they are split off from Tg and secreted into the bloodstream, under direction of thyroid-stimulating hormone (TSH or thyrotrophin). The secreted ratio of T4:T3 is usually 9:1, but because T3 is more active, 40% of T4 is converted into T3 at cells level [14].

Iodine is mainly excreted by the kidneys, after breakdown of the thyroid hormones.

2.1.1.3 Physiology

Thyroid is regulated by the TSH hormone, produced by the hypophysis, which in its turn is stimulated by TRH (thyrotropin-releasing hormone) fabricated in hypothalamus. The blood concentration of thyroid hormones also influences TSH production.

TSH influences the synthesis of hormones in the thyroid, which are stored within the follicles. 70% of these hormones enter the circulatory system attached to thyroxine-binding globulin (TBG) and the rest bound to other plasmatic proteins. The half-life of T3 and T4 is greatly augmented from this bound, resulting in a immense reservoir of circulating thyroid hormones [14].

Once inside the cell, thyroid hormones interact with cell DNA to influence regulatory genes and start the synthesis of new proteins. The newly formed proteins will mediate the cell response to thyroid hormones. Although thyroid hormones affect virtually every tissue in the body, not all have the same reaction. In most tissues the principal effect is related to metabolism, in other to growth and maturation [14, 15].

2.1.2 Pathophysiology

The thyroid gland is prone to a number of diseases that can alter its function and structure. These diseases may have wide-ranging systemic effects because, as previously said, thyroid hormones regulate the metabolism of almost every cell in the body.

Thyroid carcinoma represents the most common and prevalent of all endocrine malignancies. It is effectively treated with radioiodine therapy which associated radiation safety factors represent the focus of this work. For this reason, this disease will be described in detail below.

There are four main types of thyroid neoplasia, and some other subtypes, depending on the type of thyroid gland cells, mentioned in Section 2.1.1, from which they are developed. Papillary and follicular thyroid cancers develop from the follicular cells and grow slowly, medullary thyroid cancer develops in the C cells and anaplastic thyroid cancer develops from differentiated thyroid cancer or from a benign tumour of the gland and grows rapidly.

The first two cancers are classified as differentiated thyroid cancer (DTC), which means that the tumour tissue has the same microscopic appearance as normal tissue. Consequently, cancer cells are able to retain basic biologic characteristics, including expression of NIS and TSH receptors [20, 21]. However, some alterations in the metabolism might be present, such as: decrease in the iodine uptake and organification; shortening of effective half-life (T_e) of iodine; and decrease in Tg expression [20].

Papillary thyroid cancer (PTC, 80%) is the most common type of thyroid cancer. It is usually found in only one lobe (only 10–20% of papillary thyroid cancers appear in both lobes). Follicular thyroid cancer (FTC,10%) is less common than the first one and may occur in more advanced ages than the first one [22]. Both type of cancers represent 90% of total thyroid cancers and are very often curable, especially when found early in people under 45 years [23]. Hürthle cell cancer (HCC, 3%), is a FCT subtype, and is often classified on its own because it has a distinct histological appearance and it is often less responsive to standard therapy [12].

DTC is considered the least aggressive type of thyroid carcinoma and has, in general, an excellent prognosis. On the whole, greater than 90% of patients are alive after 10 years of diagnosis [12].

MTC has very little similarity to normal thyroid tissue and can be controlled if diagnosed and treated before it spreads to other body parts. MTC constitutes about 5% of thyroid cancers [12, 24].

Anaplastic thyroid cancer (ATC) accounts for just 2% of total thyroid cancers and represents the most aggressive tumour, most commonly found in patients from the 50–60 years age group [24]. Pathologically, ATC is grossly tan-white, fleshy, and large. During diagnosis areas of necrosis and haemorrhage are evident. Cytologically, the tumour is characterised by high mitotic activity and atypical appearing cells [25].

Between the period of 1980–2008, there have been registered an accentuated increase in the incidence of the papillary histotype, with no significant change in the other three mentioned types (Figure 2.1). The increase mainly regards small tumours, although the number of large tumours has also registered a raise [10].

2.1.3 Current Diagnosis and Treatment Options

Diagnosis is important to access whether the cancer has metastasised and which treatment may be the most effective. It may vary with patient age and medical condition, type of cancer suspected, signs and symptoms and previous test results [22].

In order to provide appropriate care based on current knowledge, there has been an attempt to standardise care to enhance the treatment of thyroid carcinoma. General guidelines were established, both in Europe [6] and Portugal [26], representing a consensus that ensure decreased mortality and protection of patient's quality of life, avoiding unnecessarily aggressive or ineffective treatments.

In Portugal [26], there was an attempt to identify prognostic factors that enabled the stratification of patients into risk groups. Patient age, tumour size, extra-thyroid extension and presence of metastases were consensually recognised. The most used prognostic scoring index is based in TNM classification, which describes the extension of a person's cancer by: T - tumour characteristics, N - lymph node involvement, and M - distant metastatic lesions. This classification was elaborated by Union Internationale Contre le Cancer (UICC) [27], and enables to assign cancer cases to low-risk or high-risk, based on factors other than the anatomic extent of the disease. 80% of the cases are considered low-risk patients [24].

A healthy thyroid gland is barely palpable. If a tumour develops in the thyroid, it might be felt as a lump in the neck. Once the presence of nodules is confirmed, biopsy is performed in order to classify a nodule as malignant or benign. As already stated, only 5% of all detected thyroid nodules are malign [6].

The general primary approach for thyroid carcinoma is surgery, followed by radioactive iodine (RAI) treatment and thyroid hormone suppression therapy [12]. The last one aims to keep TSH levels low, since they are related to stimulation of thyroid growth.

Total thyroidectomy is the preferred surgery for high-risk DTC patients, while lobectomy (the least invasive approach) is just considered for small (less than 1 centimetre) and isolated tumours. Total thyroidectomy has low surgery associated complication (below 2%) [28, 24] and has been shown to reduce recurrence rates of thyroid carcinoma [29]. This type of surgery is normally followed by radioiodine therapy that will be thoroughly assessed in the next chapter. Briefly, a remnant portion of thyroid tissue is often left after total thyroidectomy, so radioactive iodine (RAI) can destroy any remaining thyroid cells, normal or malignant [12]. This procedure is associated to better prognostics, especially in high-risk cases [30].

Treatment for MTC and ATC (tumours > 5 cm) is more controversial and might depend on the cancer nature [24] and invasiveness [31].

2.2 ^{131}I Therapy

The use of radioactive iodine (RAI) for thyroid carcinoma treatment has changed over the past 50 years [20], based on increasing understanding of ^{131}I biophysical properties and of iodine handling by thyroid cells.

RAI treatment was reported for the first time by Seidlien et al.,1948 [32], in a patient whose thyroid gland was completely removed but who was clinically hyperthyroid. This report confirmed that metastatic thyroid cancer lesions could concentrate radioiodine.

In the 1950s several groups began to evaluate the safety and efficacy associated with this therapy [33, 34, 35] and by the 1960s this treatment was already associated with increasing survival of thyroid cancer patients [36].

In the 1970s, ^{131}I therapy became popular and more available commercially, as an increasing number of studies [29, 37] were reporting good results in using ^{131}I for thyroid remnant ablation (RRA) to complete the surgical removal of all normal thyroid tissue and to destroy microscopic deposits of thyroid cancer.

Nowadays, the use of ^{131}I continues to represent a mainstay therapy for thyroid cancer due to the efficacy of this treatment which is strongly related to tumour uptake and retention.

As explained in Section 2.1.1.2, thyroid follicular cells are the only cells in the human body capable of concentrate iodide intracellularly, which is a prerequisite for radioiodine treatment, and convert tyrosine into thyroglobulin (Tg) as a substrate for thyroid hormone synthesis. Thereby, the surgical removal of all normal thyroid cells, gives the indication that the only remaining source of Tg production is malignant thyroid cells, which makes serum Tg a more specific tumour marker. In addition, any subsequent retention of radioiodine would be resultant of residual thyroid cancer [20]. Since radioiodine decays in a radioactive process, the energy emitted is responsible for easily destroying the remnant malignant thyroid cells.

Data suggest that RAI decreases disease progression and mortality [38] in high-risk patients. However, in low-risk patients the benefits of RAI are still uncertain, which requires the treatment to be used selectively. In addition, the growing awareness of its short- and long-term consequences, including damage to salivary glands, bone marrow, and gonads, especially when given in high and cumulative doses and ineffectiveness when treating advanced metastatic thyroid carcinoma demands for a more cautious and conservative approach [12]. The future role of RAI therapy strongly depends on expanding knowledge of its relative risks and benefits which will be discussed below.

2.2.1 Radioisotope

2.2.1.1 Production

Iodine-131 (^{131}I) or radioiodine is an important radioisotope of iodine that can be produced on large scales either from tellurium (Te) or from uranium (U).

Most ^{131}I results from neutron-irradiation of a natural tellurium target. The heaviest isotope, ^{130}Te, absorbs a neutron to become ^{131}Te, which β-decays into ^{131}I with a half-life of 25 min [39]. A tellurium compound can also be irradiated while bound as an oxide to an ion exchange column. In order to obtain ^{131}I, iodine can be separated from the tellurium targets by dry or wet distillation followed by dissolution in an alkaline solution [40].

^{131}I can, as well, result from nuclear fission of ^{235}U resulting into fission fragments, ^{131}I and other iodine isotopes [2]. This technique requires elaborate equipment, purification and waste handling procedures, and for this reason, it is the less employed [40].

2.2.1.2 Physical and Chemical Characteristics

The chemical properties of radioiodine are similar to the stable iodine's properties [1] so, consequently, it is involved in the same metabolic and physiologic processes that were thoroughly described in Section 2.1.1. This is one of the main reasons why thyroid cancer treatment with radioiodine is so effective since thyroid cells, normal or carcinogenic, cannot distinguish between the unstable and the stable form of iodine.

Radioiodine is highly volatile and soluble in water (0,034g/100ml at 25°C). Its melting point is at 113°C and the boiling point at 184°C [41]. Thus, pure ^{131}I is a black-violet coloured crystalline solid at room temperature, but because it readily combines with other elements, radioiodine is usually found as a compound rather than its pure form. When ^{131}I is released into the atmosphere, it often bounds chemically to hydrogen and oxygen or methane in gaseous form [42].

^{131}I has 78 neutrons and 53 protons in its nucleus and a half-life ($t_{1/2}$) of 8,0233 days [43]. During ^{131}I decay, 90% of the radiation is delivered by β^- particles ($^{131}I \rightarrow \beta^- + {}^{131}\text{Xe}^\star$) and 10% by γ emission ($^{131}\text{Xe}^\star \rightarrow \gamma + {}^{131}\text{Xe}$), transforming ^{131}I into the stable ^{131}Xe (Xenon).

The maximal energy emitted during β decay is 807 keV and the minimum energy is 248 keV, but 89% is 606 keV. After emission of β^- particles, the excited daughter nuclei ($^{131}\text{Xe}^\star$) undergo further adjustment with emission of γ-rays, between 80 and 723 keV, with 82% abundance of 364 keV [43]. The detailed decay scheme of radioiodine can be consulted in Appendix A, Figure A.1.

In the thyroid gland the biological half-life (T_b - amount of time required for the organism to remove half of the initial administered dose via biological excretion pathways) of iodine is about 120 days [44, 43]. Consequently, the effective half-life (T_e - period of time in which half of the administered dose is removed by both normal excretion and radioactive decay) of radioiodine, calculated from

$$T_e = \frac{t_{1/2} \cdot T_b}{t_{1/2} + T_b}, \tag{2.1}$$

is 7,52 days [45]. For other organs and tissues, it is assumed that organic iodine is retained with a T_b of 12 days [46], which results in a T_e of 4,81 days. Thus, two processes act to reduce the total activity in the thyroid gland: physical decay of ^{131}I represented by its physical half-life ($t_{1/2}$) and biological elimination, which depends on the metabolic activity of the cells, represented by biological half-life (T_b).

The gland picks up iodine very rapidly and because γ radiation is highly penetrable, γ activity in the gland can be detected a short time after a dose is administered. However, twenty-four hours after administering of RAI, it already corresponds to 12 to 40% of initial dose [47]. The majority of γ rays leave the patient via the skin surface, radiating the patient and the environment. Therefore, the damaging effects to the cancer cells result mainly from the interaction of β particles with cells. In fact, the harm is restricted to thyroid cells (Figure 2.6), due to the minimal penetration of β

particles in soft tissue (approximately 1 mm) [48, 44]. For these electrons, LET is approximately 0,25 keV/μm [49]. As will be explained in Chapter 3, this damage affects the DNA chain and either it is impossible to repair or the double strand is repaired incorrectly, leading to cell death while trying to activate mitosis. Many healthy and malignant cells undergo radiation-induced apoptosis [44].

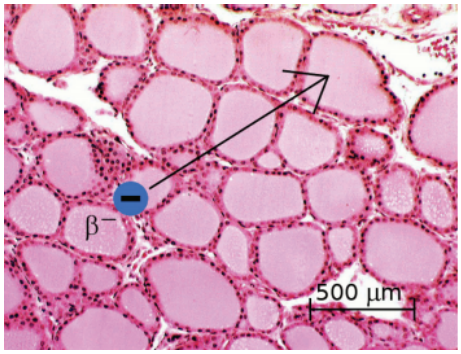

Figure 2.6: Penetration of the particle β^- in the thyroid tissue which is up to 1 mm (from [48]).

2.2.2 Procedure

^{131}I administering should be preceded by a total thyroidectomy. 4–6 weeks after surgery, if a ^{131}I scintigraphy reveals residual tumour in the neck region or distant metastases, the patient is referred to thyroid remnant ablation (RRA) [26].

RRA refers to the postsurgical administering of ^{131}I , in order to destroy any residual thyroid tissue, based on the assumptions that it may decrease the recurrence and the mortality rate [26, 29, 37] and facilitate the early detection of recurrence based on serum Tg measurement.

In normal conditions, thyroid cancer cells absorb from the blood only minor quantities of radioactive iodine that would not be enough to destroy all the malignant cells. However, when TSH is elevated, the iodine uptake capacity of these cells increase substantially [22]. For this reason, a thoroughly preparation of the patient is needed, before addressing the patient to RRA.

Traditionally, preparation for RRA involves a low-iodine diet (<50 μg/day) and withholding LT4 (levothyroxine) thyroxine replacement to increase endogenous TSH secretion, thereby stimulating iodine uptake and release of serum Tg by thyroid cells. Usually, patients are referred for the treatment when TSH concentration has risen to 25–30 μU/mL [20, 26]. It is believed that this TSH level increases NIS expression thereby contributing to an optimisation in radioiodine uptake [50]. However, this procedure is usually associated to a state of hypothyroidism that may affect patient's quality of life.

As an alternative, recombinant human thyrotropin (rhTSH) might be used in order to trigger the same effect, originating significantly fewer symptoms of hypothyroidism [51]. Side-effects are associated with mild and transient nausea or headache [51].

^{131}I is available for oral ingestion (liquid solution or in capsules) as sodium iodine (NaI) of high specific activity [44, 20], although it may also be administered intravenously in patients who are unable to ingest the radioisotope. Capsules are safer than liquid solutions since less radioactivity is released into the air during handling due to a reduction in volatility provided by the gelatin coat. In addition, capsules also cause less oral mucosal irritation [20].

Apart from the thyroid gland, the normal biodistribution of iodine include salivary glands, stomach, intestine and urinary tract, as can be seen in Figure 2.7, which means that these areas receive relatively high doses during therapy. Even though ^{131}I is rapidly absorbed, simultaneous ingestion of large quantities of water attenuates the radiation dose that may be emitted to the gastric and intestine walls during dissolution of the capsule. The major excretion pathway of ^{131}I

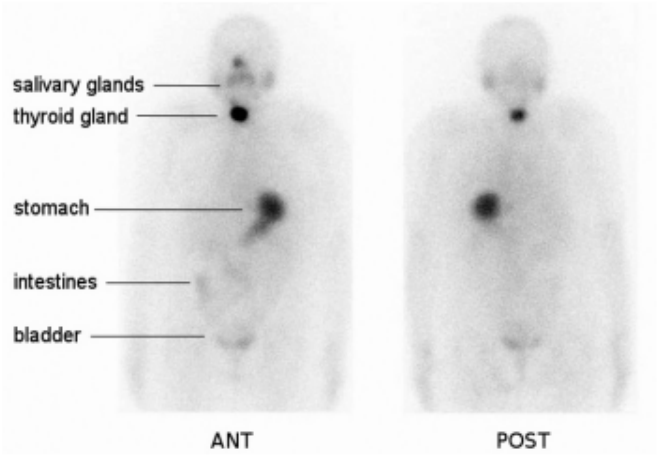

Figure 2.7: Physiological uptake of ^{131}I: anterior (ANT) and posterior (POST) views (from [44]).

is via urine. If a patient consumes 3–4 L/day of water, most of the radionuclide will be expelled in the first 48 hours [52]. However, ^{131}I may also be excreted by other means such as saliva, where it may reside for 7 days.

The main side effect of ^{131}I is the high incidence of early and late hypothyroidism [53], however occurrence of bone and soft tissue, colorectal and salivary gland cancers are also associated to ^{131}I exposure [54]. Administration of ^{131}I is strictly contraindicated in pregnant women, since cells in the process of division, such as the fetus, the bone marrow and the intestinal lining, are more likely to be induced into apoptosis than cells in a quiescent state [55]. In next section, radiation interaction with the biological tissue will be analysed in more detail. For cumulative activities higher than 18,5 GBq (or 500 mCi), the risk of leukaemia is significantly increased [20]. Nonetheless, the most clinically evident side effects of treatment with ^{131}I are usually minimal and transient. Thus, the treatment conditions should optimise the radiation dose delivered to normal and neoplastic thyroid tissues and minimise the radiation dose delivered to others in the vicinity of the patient. The latter aspect represents the main focus of this work and will be assessed in detail in the next Section.

Chapter 3

Radiological Protection

Before addressing the radiation shielding topic in detail, it is important to understand the hazards related to radiation emission, in particular during ^{131}I decay, and why there is a huge concern in blocking, or at least attenuating, its propagation.

Radiation safety is an essential topic associated with the treatment of thyroid carcinoma patients with ^{131}I.

This chapter defines the main concepts that govern the radiation exposure and interaction with matter.

3.1 Radiation Interaction With Matter

As already highlighted in Section 2.2.1.2, radioiodine decays by β^- emission followed by γ decays of the daughter nuclides. The β emission delivers the major radiation dose to the thyroid tissue, whereas the γ emission may pose an external source of radiation exposure to individuals who come into close contact with the patient. When these particles strike a target, different interactions may occur as explained below.

3.1.1 Charged Particle Interaction

Each charged particle is surrounded by its Coulomb electric force field, which interacts with the atoms it encounters as it traverses matter. In each interaction, the energy transfer, from the charged particle to matter, is generally small, which means that the particle undergoes a large number of interactions before its kinetic energy is expended. This gradual loss of energy is described by the stopping power, which depends on the charged particle's (mass, charge, velocity and energy) and on the absorber's (density ρ and atomic number Z) characteristics.

When the interaction occurs with atomic electrons it is called collision loss, which causes excitation and ionisation of the atoms; when it happens with the nucleus it is called radiative loss and energy is transferred to photons by emission of bremsstrahlung, which only light charged particles experience [3, 55].

The charged particle's path may be altered in each interaction (elastic or inelastic scattering), behaviour that is more pronounced for light charged particles. Scattering refers to the deflection of the particle from its original trajectory following an interaction. Elastic scattering occurs when the total kinetic energy is unchanged, while inelastic implies loss of kinetic energy [2].

As a result of multiple scattering events with very large scattering angles, electrons follow tortuous paths in matter [2, 3]. The biologic consequence of this non-uniform ionisation path can be quantified by the linear energy transfer (LET), which is the amount of energy deposited in matter by a charged particle as it travels through it (expressed in eV/cm) [2]. Radiations with low LET, such as electrons and β^- particles, are less dangerous to tissue [2].

3.1.2 Photon Interaction

When traversing an absorbing medium, photons experience numerous interactions with the atoms of the medium that may involve their nucleus or the orbital electrons. The type and probability of each interaction depend on the photon's energy, $h\nu$, and on the absorber's atomic number Z and density ρ. Among all the known photon interactions, only four of these are of importance to medical physics, and for this reason, will be given special emphasis in this report.

After each interaction, the photon may disappear (that is, completely absorbed) and its energy transferred to light charged particles (electrons and positrons); or scattered. If the scattered photon has the same energy as the incident photon, no light charged particle is released; if the resulting scattered photon has lower energy than the incident one, then the energy excess is transferred to a light charged particle [3]. In its turn, the light charged particle loses its energy following the interactions mentioned before (see Section 3.1.1).

Photoelectric effect

This interaction occurs between a photon and a tightly bound orbital electron of the absorber medium atom. A tightly bound electron is an electron whose binding energy E_B is comparable to, larger or slightly smaller than the photon energy $h\nu$ [3].

In the photoelectric effect, the incident photon energy is completely transferred to the electron, which is ejected from the atom with a kinetic energy $E_K = h\nu - E_B$ [2]. Hence, the photon is absorbed and the electron is now called a photoelectron. The vacancy in the shell is then filled with a higher orbit electron. The difference in energy between the two transition states is emitted either in the form of a characteristic (fluorescent) photon or in the form of an Auger electron [3].

The lower the photon energy and the higher the atomic number Z of the absorber, the more favoured is the photoelectric effect [56].

Compton scattering

The incident photon interacts with an outer shell electron, resulting in electron ejection and change in the trajectory of the photon with some reduction in energy.

The scattering angle θ (angle between the directions of the incident photon and the scattered photon) can range from $\theta = 0^\circ$ (forward scattering), through $\theta = 90^\circ$ (side scattering) to $\theta = 180^\circ$

(back scattering). When $\theta = 0°$, the energy of the scattered photon equals the energy of the incident photon, hence no energy is transferred to the electron. Therefore, it is a classical Thomson scattering [3]. Thomson scattering is a photon-orbital electron interaction, where the electron is a loosely bound electron. A loosely bound electron has a small binding energy E_B in comparison with photon energy $h\nu$. This results in an elastic scattering of the photon.

In Compton scattering, when low energy photons ($h\nu < 10$ MeV) interact, most of the energy goes to the scattered photon instead of going to the recoil electron. This is the case of iodine γ-ray photons, whose maximal energy is 723 keV. When high energy photons interact, the opposite happens.

This interaction represents the predominant interaction of γ-ray photons with soft tissue [2].

Rayleigh scattering

In Rayleigh scattering, the incident photon, normally with low energy, interacts with the whole atom of the absorber, usually with high Z. As result, a photon with exact same energy, but with different direction, is emitted. The higher the Z, the higher the scattering angle θ. However, θ decreases with increasing photon energy, $h\nu$. As all the orbital electrons contribute to the scattering event, it is referred as coherent scattering.

Because no electrons are ejected, following this interaction, ionisation does not occur [2]. Therefore, the atom is neither excited nor ionised and after the interaction, the bound atomic electrons revert to their original state.

Pair production

Pair production occurs when a high energy photon interacts with the Coulomb field of an atomic nucleus or orbital electron. As a result, the photon's energy is transformed into an electron-positron pair [3]. Hence, the photon is completely absorbed and its energy transformed into mass.

Pair production is followed by annihilation of the positron with an orbital electron of the absorber.

The probability for pair production increases with the incident photon energy, especially in higher Z materials [56].

3.1.3 X-ray Production

As charged particles and photons interact with matter, secondary X-rays production may occur. There are two principal methods that are explained below.

Characteristic X-rays

When there are left vacancies in the lower shells, either by ionisation of inner electrons or through excitation of electrons to higher energy levels, the electrons begin a series of transitions until the ground state of the atom is achieved.

The discrete energy correspondent to the difference in the binding energy between the final and initial states is either emitted as a photon, a characteristic X-ray, or ceded to an outer electron,

which is ejected from the atom and for that it is called an Auger electron. Each electronic transition probability depends on the Z number of the atom and, thus, the characteristic X-rays provide a unique signature for each element [55].

Bremsstrahlung

As previously said (see Section 3.1.1), charged particles stopping power can be of two types: collision loss or radiative loss. In the last case, the photons produced are called bremsstrahlung (literally "braking radiation") [55].

Bremsstrahlung is more relevant for light charged particles with high energy in high-Z material [3, 55].

3.2 Radiation Field

Radiation field refers to all the particles and their trajectories in some region of space or through some boundary, either per unit time or accumulated over a certain period of time [55].

This section describes how to characterise a radiation field in terms of radiometric and dosimetric quantities, according to national legislation and Shultis et al., 2010 [55]. Radiometric quantities are not enough related to most of the radiation effects to be a useful determinant. Therefore, dosimetric quantities are used with the purpose of correlating a physical measure with a radiation effect.

3.2.1 Radiometric Quantities

Fluence

In a radiation field, fluence Φ is defined as the number of particles, dN, penetrating into a sphere of cross-sectional area, dA, as

$$\Phi = \frac{dN}{dA}. \tag{3.1}$$

Fluence rate

The fluence rate or flux is expressed in terms of the number of particles entering a sphere, per unit time:

$$\phi = \frac{d\Phi}{dt}. \tag{3.2}$$

3.2.2 Dosimetric Quantities

Absorbed dose

Absorbed dose (D) is defined as the absorbed energy per unit mass, in gray (Gy),

$$\mathrm{D} = \frac{dE}{dm}, \tag{3.3}$$

where dE is the mean energy imparted to the matter by ionising radiation in a volume element and dm is the matter mass in the volume element. This is a very useful concept in radiation protection, since energy imparted per unit mass in tissue is very closely correlated with radiation hazard. However, D does not provide information about the total mass of tissue exposed and/or distribution of the absorbed energy.

Equivalent dose

The equivalent dose (H_T), in sievert (Sv), is the absorbed dose by the tissue or organ, weighed by the radiation type R, according to,

$$H_T = w_R D_{T,R}, \tag{3.4}$$

where $D_{T,R}$ is the mean absorbed dose by the tissue or organ T and w_R is the weighing factor concerning to the radiation type. For photons (γ) and electrons (β^-) emission, the radiation weighing factor (w_R) is 1, thus concerning ^{131}I therapy, the equivalent dose (H_T) equals the absorbed dose (D), in each tissue or organ T. In Appendix B, Table B.2 presents the weighing factors for other radiation types, obtained from Directive L 013, OJEU, on 17th January 2014 [4].

When the radiation field is composed by different w_R values, the total equivalent dose is given by the summation of individual equivalent doses, H_T.

Effective dose

The effective dose (E_D), in sievert (Sv), is obtained from the summation of the equivalent doses (H_T) to each organ or tissue and its respective weighing factor (w_T), according to

$$E_D = \sum_T w_T H_T, \tag{3.5}$$

thus representing the total body radiation risk. The tissue weighing factor (w_T) for thyroid gland is 0,04. In Appendix B, Table B.1 presents the weighing factors for some others organs and tissues, obtained from Directive L 013, Official Journal of the European Union (OJEU), on 17th January 2014 [4].

Kerma

Kerma, K, is an acronym for kinetic energy of radiation produced per unit mass and takes the form:

$$K = \frac{d\overline{E}_t r}{dm}, \tag{3.6}$$

where $d\overline{E}_t r$ is the average energy transferred to the secondary charged particles, as a result of photon interaction in matter of mass dm.

Under charged particle equilibrium, which exists when in an incremental volume, for every

charged particle with a certain kinetic energy leaving the volume, another with the same characteristics enters the volume, absorbed dose and kerma are equal. This condition is closely achieved in many practical situations [55].

Exposure

Exposure, X, is related to the ability of photons to ionise air and thus used to specify the radiation field of γ and X-ray photons. It is defined as the absolute value of the ion charge of one sign, dQ, produced anywhere in air by the complete stoppage of all light charged particles, except those produced by bremsstrahlung, that are liberated in an incremental volume of air, per unit mass of air in that volume, dm_{air} [55], then

$$\mathrm{X} = \frac{dQ}{dm_{air}}. \tag{3.7}$$

The SI unit is coulombs per kilogram (C kg^{-1}).

Exposure and kerma in air are closely related, however, while K measures the kinetic energy of the secondary electrons, X measures de ionisation caused by interaction of those electrons with air.

Exposure rate constant

Exposure rate constant (ERC or Γ), characterises the energy transferred to the air by the photons emitted by a radioactive source. This quantity can also be called specific gamma ray constant, among a variety of other names.

For a particular point source of radioactivity, Γ relates its associated activity (A) to the exposure dose rate ($\delta D/\delta T$) in air, at a given distance (d) from the source:

$$\frac{\delta D}{\delta T} = \Gamma \frac{A}{d^2}. \tag{3.8}$$

3.3 Health Physics

In this section, the absorbing medium is assumed to be the biological tissue. As radiation passes through it, interactions with ambient atoms occur, leading to chemical free radical production that may react with cell biomolecules. The damage extent of these reactions on the cells and how they affect the organism is not easily determined and this is the reason why radiological protection measures should be implemented.

The biological effects of ionising radiation (IR) depends on both exposure and duration of exposure [55]. The cumulative exposure may trigger two types of biological effects: deterministic and stochastic. The first are caused by acute, life-threatening exposure leading to a decrease or loss of organ function due to cell damage or death. The high energy content in IR is strong enough to disrupt chemical bonds throughout the cell, damaging the DNA molecules and leading to cellular dysfunction and ultimately cell death [20]. Cell death is triggered when damage in the double

strand of DNA is repaired incorrectly or it is not repaired at all. Thus, when trying to activate mitoses, cells undergo apoptosis, that is, natural programmed cell death.

However, a pathological dysfunction is only clinically observable when a large number of cells is damaged, so it is possible to define a threshold, from which the effects are visible [57]. For example, the aim of thyroid cancer treatment is to destroy remnant thyroid tissue while not affecting other organs in such a way that deterministic effects occur. This is possible due to the capacity of thyroid cells to take up iodine.

Stochastic effects result from alterations in cells that retain their ability to divide, from minor acute or low-level exposure. These modifications initiate a malignant transformation leading to the development of a malignant clone and eventually to a clinically observable cancer. If germ cells are irradiated, genetic effects may result [57]. For stochastic effects no threshold dose is assumed and the probability of their occurrence is proportional to the dose, which should be kept as low as possible. Effective dose (E_D) is the most common dose measure used for comparing the risk of stochastic effects (See Section 3.2.2).

Following ^{131}I decay both β-particles and γ-rays are emitted. The first particles represent the highest contribution to the success of the treatment, while the majority of the second ones, leave the patient via the skin surface. The predominant interaction of γ-ray photons with soft tissue is by Compton scattering [2].

Because virtually no β-particles escape from large tumor deposits where ^{131}I is concentrated, large doses of ^{131}I may be given without damaging surrounding tissues. In addition, due to the surgical removal of thyroid tissue, elimination of radioactivity resultant from the administration of ^{131}I occurs at a faster rate, thereby allowing higher doses treatments [58]. However, from a radiation protection point of view, the best strategy is to always use a radiation dose as low as possible that will not compromise the desired effects and benefits for patients.

Studies show that 53% of patients achieved ablation after a single administration of ^{131}I up to 1110 MBq (30 mCi). This value increases up to 86% if the activity of the administered dose corresponds to 3700 MBq (100 mCi) [59]. Currently, standard therapy with ^{131}I is given as fixed doses or activities. Small cancers confined to thyroid may receive the lowest dose (1110 MBq or 30 mCi) while more advanced cancers with metastases at distance receive higher doses (up to 7400 MBq or 200 mCi) [6, 26].The retained activity, however, changes over time. This quantity depends on the administered activity, the mass and function of the thyroid tissue and the rate of clearance, that can be stimulated by patient's hydration and renal function [52].

After the administration, the patient is kept in an isolated unit with a single-bed with dedicated toilet and ablution facilities, until the radiation dose rate drops below 30 μSv/h [60]. This amount is strongly influenced by thyroid mass, patient orientation and biodistribution of the radiopharmaceutical within the organism (see Figure 2.7) and should be measured with a portable survey meter held at a distance of 1 m anterior to the patient's neck. Notwithstanding, radiation exposure may also result from contacting with ^{131}I that was secreted by the treated patient. The majority of

the excretion occurs via urination, but small amounts of the radionuclide may also be present in saliva, tears and other body fluids.

Exposure rates should also be measured in strategic points, such as, at the bedside, at the doorway and in the neighboring rooms of the hospital unit in accordance with the occupancy factor (present in Table 3.1).

Table 3.1: Occupancy factor relative to members of the public [61].

Value	Occupation
1	Areas with total occupation
1/4	Areas with partial occupation
1/16	Areas of occasional occupation

Total body retention or external radiation dose rate should thereby be measured before discharge of the patient, to ensure that regulatory criteria for radioprotection are met, that will be explained thoroughly in the next section.

3.4 Review of National Regulation

The European Atomic Energy Community (EURATOM) established basic safety standards related to the health protection, of workers and members of the public, against the dangers arising from ionising radiation, that were adopted by Portuguese national legislation.

According to D.L. n^{o}165/2002, on 17th July 2002 [62], an "exposed worker" is a person, either self-employed or working under an employer, subjected to exposure at work from practices covered by the mentioned Directive, that are likely to result in doses higher than the fixed threshold dose established for the members of the public. In D.L. n^{o}222/2008, on 17th July 2008 [63], which is in accordance with Directive L 013, Official Journal of the European Union (OJEU), on 17th January 2014 [4], the effective dose (E_D) threshold for exposed workers is established as 100 mSv per five years in a row, provided that this amount does not exceed the maximum value of 50 mSv in each year. For a member of the public the limit dose is 1 mSv per year. This information is summarised in Table 3.2. In case of pregnancy, the limit should not exceed 1 mSv during the pregnancy period, especially for the unborn child.

Table 3.2: Effective dose threshold (E_D, in mSv) for exposed workers and members of the public, per year and for a period of 5 years in a row [63].

	1 year	5 years
Exposed worker	50	100
Member of the public	1	5

Concerning partial body exposure, the equivalent dose (H_T) threshold for the lens of the eyes, skin, hands, forearms, feet and ankles are also established in the same Directive for both exposed workers and members of the public, which can be consulted in Table 3.3.

Table 3.3: Equivalent dose threshold (H_T, in mSv) for exposed workers and members of the public, for a period of 1 year [4].

	Eyes' lens	Skin	Hands, forearms, feet and ankles
Exposed worker	50	500	500
Member of the public	15	50	

A unit intended for the administration of radiation for therapy, should also obey to dose constraints, according to the same Directive. Therefore, a distinction shall be made between supervised areas and controlled areas. That is, areas in which it is possible that exposure to which workers are subjected can exceed one-tenth (from 2 to 6 mSv/year) or three-tenths (from 6 mSv/year), respectively, of the dose limits established for exposed workers. Therefore, supervised areas are planned for members of the public and non-exposed workers and controlled areas for exposed workers. For the first one the limit is 1 mSv/year or 0,02 mSv/week and, for the second one, the limit is 20 mSv/year or 0,4 mSv/week (Table 3.4).

Table 3.4: Dose limit (mSv), per week and per year, for controlled areas and supervised areas [4].

	1 week	1 year
Controlled area ($\Rightarrow$ Exposed worker)	0,4	20
Supervised area ($\Rightarrow$ Member of the public)	0,02	1

According to D.L. n^{o}180/2002, on 8th August 2002 [61], a unit for inpatient therapy, beyond hospital standards, must also include rooms with radiation protection, taking into account the maximum activity estimated for each room. These rooms must comprise a single bed, toilet and restricted furniture easy cleanable. After discharge of the patient, the room must be decontaminated.

In order to ensure radiation safety conditions, the design of these units should take into account the location, configuration, number of rooms and their dimensions. Adequate protection is obtained by controlling the workers distance to the radiation source, the exposure time and the existing shielding, which must take into account the proper location of the radioactive source and the type, energy and directions of the irradiation [61].

For the purpose of this work, the unit is meant to accommodate a nuclear medicine service valence, in where patients diagnosed with thyroid carcinoma will be administered with radioactive iodine, which implies hospitalisation due to the high doses applied.

3.5 Radiation Safety Factors

There are four major methods by which radiation exposure can be minimised.

Radiation levels decrease with the square of the **distance** from the point source of radiation, given by the inverse square law. Therefore, the exposure dose rate $(\delta D/\delta T)_2$ at distance d_2 is given by Equation 3.9, knowing that at distance d_1 the exposure rate from the same radioactive source is $(\delta D/\delta T)_1$.

$$\left(\frac{\delta D}{\delta T}\right)_2 = \left(\frac{\delta D}{\delta T}\right)_1 \left(\frac{d_1}{d_2}\right)^2 \tag{3.9}$$

Intuitively, radiation dose is directly proportional to **duration** of exposure, therefore exposure time should be minimised. However, the human body does not irradiate at a constant rate, thereby knowledge of both the exposure rate and how it changes over time are important elements in minimising personnel exposure.

Another factor is related to **contamination control** methods that are planned to avoid radioactive materials entering in contact with personnel and its spread. Adequate protection includes handling precautions and disposable materials. The former must be discarded into designated radioactive waste containers, so that decay to background levels is allowed. As ^{131}I is a volatile radionuclide, it should be stored in an exhaust fume hood in order to avoid air contamination and subsequent inhalation.

The last factor has a prominent role concerning the purpose of this work. The use of proper **shielding** should be used to diminish radiation exposure levels to the unit sorrouding areas. The shielding characteristics, such as material type, thickness and location, depend on the radiation type, energy and intensity, as well as, on the geometry and location of the radiation source [2]. This barrier aims to ideally block or attenuate the radiation emitted by ^{131}I after administration by the patient.

3.6 Shielding Design

After administration of ^{131}I for thyroid cancer therapy, the patient becomes a potential radiation hazard to others and should be isolated if the activity administered is higher than 740 MBq (20 mCi) and while the radiation dose rate is higher than 30 μSv/h [60].

Isolation aims to allow radiation exposure to drop to national legislation acceptable levels and below, following the ALARA principle, that is, to reduce radiation exposure to levels that are as low as reasonably achievable.

The dose limits established by national and European agencies are indicators of the maximum dose amount acceptable resultant from exposure to ionising radiation, under particular conditions. All entities are required to employ good health physics practices and radiation safety programs to ensure that radiation exposure is kept as low as reasonably achievable (ALARA). This principle

represents a commitment between both employee and employer to minimise radiation exposure to staff and general public.

Thereupon, the radiotherapeutic room should follow a judicious shielding design plan, with the goal of minimising radiation exposure to those limits highlighted in Section 3.4.

The design requires thorough characterisation of the radiation source and must consider the maximum possible dose, so the type and configuration of the necessary shielding for the most extreme situation could be determined. As it was already stated, ^{131}I emits both β^- particles and γ radiation during decay. While β particle present high ionising capability, and for this reason, successfully harming cancerous cells, γ radiation, constituted of photons, possess greater penetrating power and for this, poses an external source of radiation for others and consequently, should be blocked or attenuated.

Shield properties should be well understood as well as radiation interaction with those materials, since the type and probability of an interaction depend on the photon's energy, $h\nu$, and on the absorber's atomic number Z and density ρ. The shield design should be optimised in order to minimise weight, volume and cost. These considerations represent the exact aim of this work and will be assessed in the next sections.

3.6.1 Radiation Sources

If the volume of the source is sufficiently small, that is, if the source's dimensions are too small when comparing to the dimensions of the attenuating medium between the source and the dose point, and there is negligible interaction of radiation with the matter in the source volume, then the real source can be mathematically treated as a point source [55, 56].

A point source may depend on energy, direction and time. However, in most of the shielding practices, time is not treated as an independent variable, since the time delay between a change in the source and the consequential change in the radiation field is normally insignificant. In addition, radioisotope sources are certainly isotropic, meaning that they radiate uniformly in all directions throughout a 4π geometry, and ^{131}I is no exception. Consequently, source characterization requires only knowledge of energy. In this particular case, energy dependence is discrete.

3.6.2 Attenuation of Gamma and X-rays

Attenuation is the removal of photons from a beam as it crosses a particular material, by the interactions mechanisms already discussed in Section 3.1.2.

Briefly, when γ radiation is incident on a finite thickness of material, there is the probability that it will interact with the material and be attenuated, depending on the photon energy and on the Z number and density of the material.

Photoelectric effect, Compton scattering and pair production represent the interactions of major importance, followed by Rayleigh and Thomson scattering. When low energy photons are involved, photoelectric effect is the preferred interaction. With increasing energy, Compton scattering prevails. Only at very high photon energies ($> 1,02$ MeV) would pair production contribute

to attenuation. Rayleigh scattering plays no role in radiation dosimetry, since no energy is transferred to charged particles. Consequently, it is often ignored in shielding barrier calculations.

As a consequence of these interactions, secondary X-rays production may occur (Section 3.1.3). But, because in most shielding applications X-rays have usually energies $\leq$100 keV, they are easily attenuated by any shield adequate for the primary radiation, and hence often neglected in analyses involving higher energy photons [55].

Charged particle interactions are not considered in shielding situations, even if they were emitted by the radioactive source and its slow down in the material would produce bremsstrahlung, because the gamma and X ray photons are usually more numerous and penetrating than the bremsstrahlung.

The most important parameter used in the characterisation of gamma and X-ray penetration into absorbing media is the linear attenuation coefficient μ (typically cm^{-1}), which describes the fraction of photons removed from a monoenergetic beam of X- or gamma rays, per unit thickness. This coefficient depends on energy $h\nu$ of the photon and on the atomic number Z of the absorber.

In a homogeneous medium, the linear attenuation coefficient is constant for the same energy. It can be determined using a narrowly collimated source of monoenergetic photons that traverses a slab of absorber material with thickness x until it reaches a narrowly collimated detector (narrow beam geometry). The material decreases the initial intensity, I(0), exponentially according to Beer's Law:

$$\mathrm{I}(x) = \mathrm{I}(0)e^{-\mu x}. \tag{3.10}$$

Consequently, the exposure dose rate decrease in the same manner and Equation 3.10 can be rewritten as

$$\frac{\delta D_f}{\delta T} = \frac{\delta D_i}{\delta T}e^{-\mu x}, \tag{3.11}$$

where $(\delta D_f/\delta T)$ represents the final dose rate resultant from the attenuation of the initial dose rate $(\delta D_i/\delta T)$, as a consequence of crossing a material with thickness x, that reached the detector. Thus, $(\delta D_f/\delta T)$ is the dose resultant from the primary photons, that is, photons that crossed the material without interacting.

For a given thickness, the probability of interaction is dependent on the number of atoms per volume. In order to overcome this dependency, the linear attenuation coefficient can be normalised to unit density of the absorbing material. This coefficient is called the mass attenuation coefficient μ_m (cm^2/g). For a compound of mixture of materials, the mass attenuation coefficient is approximated by the summation of a weighted average of its constituents:

$$\frac{\mu}{\rho} = \sum_i w_i \frac{\mu_i}{\rho_i}, \tag{3.12}$$

where w_i is the proportion by weight of the i-th constituent and μ_i/ρ_i is the mass attenuation coefficient of the i-th constituent.

These coefficients have specific values for a given photon energy $h\nu$ and absorber atomic number Z, with density ρ. They result from the sum of values for all the individual interactions mentioned before, hence

$$\mu = \tau + \sigma_R + \sigma_C + \kappa, \tag{3.13}$$

$$\mu_m = \frac{\mu}{\rho} = \frac{\tau + \sigma_R + \sigma_C + \kappa}{\rho}, \tag{3.14}$$

where τ is the linear attenuation coefficient for photoelectric effect, σ_R is the linear attenuation coefficient for Rayleigh scattering, σ_C is the linear attenuation coefficient for Compton scattering and κ is the linear attenuation coefficient for pair production.

3.6.3 Characteristic Absorber Thicknesses

Mean free path is the thickness necessary to attenuate the beam intensity to $1/e = 0,368(36,8\%)$. The photon mean free path is the average distance a photon travels through a given absorber before undergoing an interaction. The thickness of the material at which the radiation intensity is reduced by half is the material's half-value layer (HVL) [64]. Similarly, the tenth-value layer (TVL) is the thickness necessary to reduce the initial intensity to a tenth of its value. By knowing μHVL and/or μTVL of a material for a given energy, it is possible to calculate the necessary thickness to efficiently shield a nuclear medicine unit, respectively, according to

$$\mu_{\text{HVL}} = \frac{\ln 2}{\text{HVL}}, \tag{3.15}$$

$$\mu_{\text{TVL}} = \frac{\ln 10}{\text{TVL}}. \tag{3.16}$$

3.6.4 Build-up Effect

In radiation protection, particularly in shielding design, it is used a broad beam geometry, in contrast to the narrow beam. In this case, the beam is not collimated and consequently, the final dose rate equals $B.(\delta D_f/\delta T)$, where B is the build-up factor that accounts for the secondary photons that are scattered from the absorber and $\delta D_f/\delta T$ the final dose rate in a narrow beam geometry. Thereby,

$$\frac{\delta D_{f_B}}{\delta T} = B\frac{\delta D_i}{\delta T}e^{-\mu x}. \tag{3.17}$$

For a monoenergetic gamma emitter, the build-up factor represents the ratio of total dose (primary and secondary photons) to the dose from primary photons alone. It is a dimensionless quantity, which magnitude varies widely, ranging from a minimum of 1, where $\delta D_{f_B}/\delta T = \delta D_f/\delta T$, to very large values, depending on photon energy and shielding characteristics (material and thickness), geometry and distance to the radioactive source [56].

According to Groth, 1998 [60], for a patient submitted to radioiodine treatment in a typical isolation room, B lies between 1,25 and 1,35 (assuming thyroid area from 400×300 mm^2 to 700×300 mm^2).

3.6.5 Shielding Materials

After source characterisation, comprehension of possible photon interactions and review of regulatory criteria concerning acceptable dose limits, there is a parameter that still needs to be taken into account that is materials' evaluation and geometry. This concerns assessment of elemental composition and densities of material components, as well as, its placement on the room. Also, according to the radiation types emitted by the radioactive source, homogeneous or layered materials might be demanded. This also represents a shield-optimisation problem where decision should be made towards number and thicknesses of the layers.

According to Directive L 013, OJEU, on 17th January 2014 [4], a building material should be designed to be permanently incorporated in a building or parts thereof, since it influences its performance regarding exposure of its occupants to IR.

Air is assumed to be a natural shielding material. Dry air, at 1 atmosphere and 20^o has a density of 0,00120 g cm^{-3} [55]. Ordinarily ideal gas laws should be applied to recalculate density for different temperature, pressure and humidity.

High density concrete is often used to provide greater attenuation for a given thickness. This is a highly desirable material since it gathers reasonable cost, compressive strength, ease of placement and effectiveness in gamma ray attenuation. Reinforcing steel provides tensile strength and adds density to concrete.

Metallic materials are also used for shielding purposes, namely lead, allow steel and stainless steel. Lead is the most frequently used shielding material, alongside with concrete. It has low strength, low melting point and high density ($\rho = 11,350$ g cm^{-3} [65]).

To sum up, β radiation emitted by ^{131}I is practically restricted to the thyroid gland and hence, will hardly reach the shielding walls. The distance between the radioactive gland and the walls is relatively large when compared to the thyroid dimensions and β particles do not have enough penetrating power to travel a distance so far.

However, primary radiation may induce secondary energetic particles as a result of the interactions processes, which in turn may also produce other particles, with lower and lower energies. Therefore, it is necessary to be aware of the dependence of the various fundamental interaction processes on particle energy and on absorber atomic number (Z), to understand these cascade processes.

Therefore, considering photon radiation, materials with higher Z numbers are necessary. The most commonly used materials for the shielding of this radiation are lead and concrete. The attenuation provided by a 190 mm core-filled concrete block wall is equivalent to a 13 mm lead

sheet for ^{131}I [66]. This evidence should be taken into consideration in the shielding optimisation assessment.

The best shielding for β particles is a double-layered shield, made by a first material with a small Z, such as plastic or glass, followed by a second material with higher Z, such as lead. This shield aims to attenuate high-energy beta radiation while minimising bremsstrahlung [2, 44].

Also, the shielding plan for a nuclear medicine unit for thyroid carcinoma therapy must consider the number of treatments to be performed, the activity of ^{131}I and the occupancy factors within the room and for adjacent areas. Protocols for thyroid cancer treatment with ^{131}I may vary from country to country and even within the same country, from hospital to hospital, however thyroid mass and biokinetics of ^{131}I in the patient thyroid should always be assessed so a more precise absorbed dose could be computed.

Chapter 4

Radiation Source Properties

4.1 Decay Analysis

Depending on the radiopharmaceutical, the production site may not correspond to the site where the radioisotope will be used.

In this work, ^{131}I was delivered to the nuclear medicine service where the suitable equipments for the measurement of the initial activity are present and only after, it was transferred to the hospital unit intended for ^{131}I administration. Therefore, it was necessary to evaluate the decay behaviour of the radioisotope, within the actual conditions, to be certain that it followed the theoretical assumptions, since this information will be needed in future considerations. This experimental decay analysis was performed for three radioisotopes (^{99m}Tc, ^{67}Ga and ^{131}I) that will be used in posterior experiments. This procedure was necessary since the radiation sources were transferred to the site where the measurements were held after production in a different location.

A priori, the known physical characteristics of interest for each radioisotope were gathered and assumed as the reference values (Table 4.1), with which the determined experimental values were compared.

Table 4.1: Physical characteristics relative to ^{99m}Tc, ^{67}Ga, ^{131}I decay [43].

Radionuclide	$t_{1/2}$	λ
^{99m}Tc	6,0067 h	0,1154 h^{-1}
^{67}Ga	3,2613 d	0,2125 d^{-1}
^{131}I	8,0233 d	0,0864 d^{-1}

Briefly, ^{99m}Tc half-life ($t_{1/2}$) is 6,0067 hours and the decay constant (λ) is 0,1154 h^{-1} [43]. As already explained, these quantities can be related by Equation 1.3. ^{67}Ga has a $t_{1/2}$ of 3,2613 days, and therefore, a λ of 0,2125 d^{-1} [43]. ^{131}I has a radioactive decay half-life of 8,0233 days [43], which means a decay constant of 0,0864 d^{-1}.

The activity of the radionuclides was measured at different times: immediately after preparation ($A(0)$) and throughout the measurement ($A(t)$), with recourse to two different dose calibrators: Dose Calibrator 1 (DC1) - PTW, Curiementor 3, s.n. 1110731, with manufactured data at March, 2001 - and Dose Calibrator 2 (DC2) - LemerPax, Posidose, s.n. 00905, with manufactured data at June, 2010. DC1 registers the activity in its vicinity, so there is the need to acquire the residual activity and then subtract this value to $A(t)$. The second dose calibrator does this calculation automatically after manual calibration every time a measure is performed. This is the main difference between the two dose calibrators. Both calibrators have an associated error of $\pm$0,00005 mCi.

The results were manipulated with Excel®, according to

$$\ln A(t) = \ln A(0) - \lambda t, \tag{4.1}$$

where $A(0)$ represents the initial activity, at time $t = 0$, $A(t)$ the measured activity at the time t the values were registered and λ the experimental decay constant for each dose calibrator. This expression results from the manipulation of the fundamental decay equation (Equation 1.2) that shows the exponential radioactive decay. The minus sign indicates that the number of radioactive atoms decaying per unit of time decreases with time. Following the logarithmic representation, λ is easily identified as the slope of the curve. For each radioisotope, the experimental λ is the average of the decay constants obtained from the measurements performed with the two dose calibrators followed by application of appropriate unit conversions. The respective half-life ($t_{1/2}$) was obtained after application of Equation 1.3.

As expected, the plot of the activities as a function of time results in an exponential relationship in which the total activity asymptotically approaches zero (in Appendix C in Table C.1 – Table C.3). Graphical representations were obtained following representation of Equation 4.1, as can be seen in Appendix C in Figure C.1 – Figure C.3.

Both tabulated and experimental values, as well as the associated relative error, are shown in Table 4.2. All the obtained experimental values are in accordance with literature [43], despite a minimum deviation that may be justified by the degree of sensitivity of each calibrator and due to the influence from the natural background radiation that is also present in the fume hood where the measurements were held.

Table 4.2: Experimental half-life time ($t_{1/2}$) and decay values (λ) and the error relative to the tabulated values [43].

	^{99m}Tc		^{67}Ga		^{131}I	
	$t_{1/2}$	λ	$t_{1/2}$	λ	$t_{1/2}$	λ
Tabulated	6,0067 h	0,1154 h^{-1}	3,2613 d	0,2125 d^{-1}	8,0233 d	0,0864 d^{-1}
Experimental	5,9872 h	0,1158 h^{-1}	3,3134 d	0,2092 d^{-1}	8,4082 d	0,0825 d^{-1}
$\pm$ Relative error (%)	0,3245	0,3393	1,5975	1,5529	4,7978	4,5718

As the difference between reference and experimental values of λ and $t_{1/2}$ for all the radionuclides is too narrow to be considered, the production of the radionuclides and acquisition of initial activity in an external nuclear medicine service followed by transfer to the therapy unit is suitable for the posterior measurements.

4.2 Exposure Rate Constant Determination

The exposure rate constant (ERC or Γ) is an important factor needed for routine calculation in medical physics regarding radiation safety and medical uses of radionuclides, since it characterises the energy transferred to the air by the photons emitted by a radioactive source. For an isotropic point source of gamma radiation, the ERC is given by Equation 3.8, where it is denoted by Γ. The purpose of this step was to determine experimentally the ERC for ^{99m}Tc, ^{67}Ga and ^{131}I, in order to comprehend which factors affect this quantity and in which amount. A theoretical calculation was also performed, according to Smith and Stabin method [67], for comparison purposes. Since published data may present some disagreement, this quantity was recalculated in this work from recently updated data.

4.2.1 Theoretically

According to Stabin and Michael, 2007 [68], in terms of the decay spectrum of a nuclide, ERC can be written as

$$\Gamma_\delta = \frac{1}{4\pi}\sum_i \left(\frac{\mu_{en}}{\rho}\right)_i Y_i E_i, \tag{4.2}$$

where μ_{en}/ρ represents the mass-energy absorption coefficient in air for photons of energy E emitted by the nuclide, during the decay process, with a certain yield Y. i corresponds to each photon energy, which contribution must be summed up. δ is the minimum cut-off energy. This value determines the minimum energy photon that can contribute to the exposure.

All the characteristic energies E_i of the emitted photons and their corresponding yields Y_i were obtained from NuDat 2.6, which is a database developed by the National Nuclear Data Center [69]. More specifically, information about ^{99m}Tc was originating from Browne and Tuli, 2011, [70]; about ^{67}Ga from Huo et al., 2005, [71]; and about ^{131}I from Khazov et al., 2006, [72]. As in Smith and Stabin, 2012 [67], only values equal or above 15 keV ($\delta = 15$ keV) and yields of at least 10^{-4} were considered. The reason for neglecting these energies is due to the fact that in practice, these emissions almost never contribute to dose given the rapid attenuation of these photons [67].

The μ_{en}/ρ for the photons with energy E were taken by interpolation of Hubbell and Seltzer, 1996, [65] data.

The appropriate unit conversions were applied so the final units were (μSv m^2)/(MBq h).

Comparison of ERC values, for the selected radionuclides, calculated theoretically to those from Smith and Stabin, 2012 [67], Unger and Trubey, 1982 [73], Tschurlovits et al., 1992 [74] and Ninkovic et al., 2005 [75] is shown in Table 4.3.

Table 4.3: Comparison of the calculated ERC values for the selected radionuclides.

Exposure rate constant (μSv m^2)/(MBq h)				
Radionuclides	This work	Smith and Stabin, 2012 [67]	Unger and Trubey, 1982 [73]	Ninkovic et al., 2005 [75]
^{99m}Tc	**0,020084**	0,020600	0,033200	0,014100
^{67}Ga	**0,019949**	0,020800	0,030000	0,019450
^{131}I	**0,055197**	0,056500	0,076400	0,052200

The values obtained in this work were generally lower than the values found in the literature, except for Ninkovic et al., 2005 [75]. The reason for the lower values obtained by Ninkovic et al., 2005, is probably justified by the fact that its method only considers photon energies above 20 keV.

Relatively to Unger and Trubey, 1982 [73] because they included emissions down to 10 keV, the resultant values were higher than the ones obtained in this work. Also, instead of using absorption coefficients, Unger and Trubey used a fitted function of dose rate per unit flux density.

Therefore, the difference in the results may be related to differences in methodology. The higher the minimum cut-off energy (δ), the lower the ERC value.

The ERC values obtained in the present work are very similar to the ones provided by Smith and Stabin, 2012 [67], since they were calculated following the same methodology. Minor variations arise from differences in source data.

4.2.2 Experimentally

The experimental determination of ERC was conducted in a wide open area, without near barriers, for each radionuclide with initial activities present at Table D.1. The radioactive decay was taken into account based on the assumptions presented in Section 4.1.

The exposure dose rate ($\delta D/\delta T$) was acquired at strategic points, according to Figure 4.1, with a portable dosimeter (AT1121, Atomtex®- see Appendix E for detailed specifications) enabled to acquire X and gamma radiation every second. By knowing the distance d between the radioactive source and the dosimeter and the activity at the time of the measurement $A(t)$ (Equation 1.2), the calculation of Γ was direct, following transformation of Equation 3.8:

$$\Gamma = \frac{d^2}{A(t)}\frac{\delta D}{\delta T}. \tag{4.3}$$

The first round of measurements was performed with the radioactive source placed at 1 m from the floor (Figure 4.1a).

In order to quantify the influence of the increasing distance, d, the measurer was placed at 1 m (P1, P4, P7), at 2 m (P2, P5, P8) and at 3 m (P3, P6, P9) from the source, at the same height. For each distance, measurements were acquired in three different points, with the purpose of studying the horizontal angular influence: at 0^o (P1, P2, P3), at 120^o (P4, P5, P6) and at 240^o (P7, P8, P9).

The vertical angular influence was also accounted by measuring the dose rate, relatively to the source height, at -46^o or 0 m height, that is, on the floor (P10, P11, P20) and at 25^o or 1,5 m height (P12, P13).

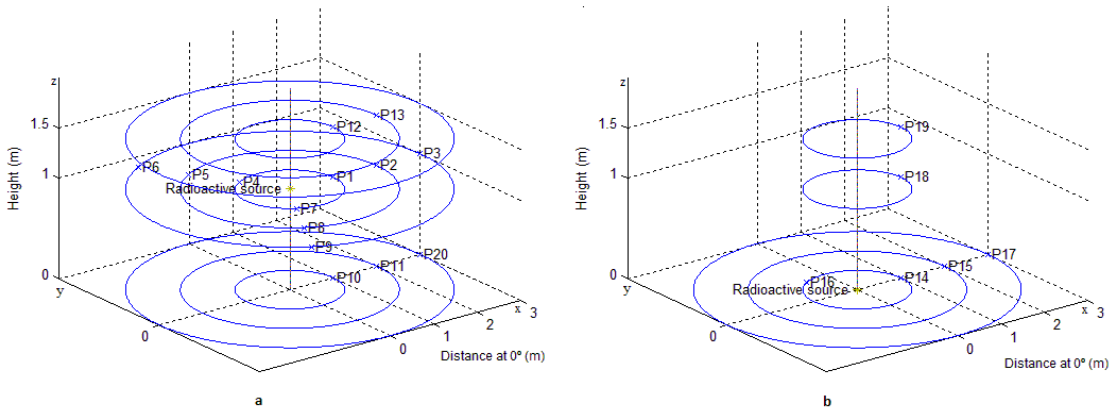

Figure 4.1: Distribution scheme of the measurement points with the radioactive source placed at a) 1 m from the floor (z=1) and b) on the floor (z=0). The schemes were obtained using Matlab.

The second round was performed with the radioactive source placed on the floor (0 m height), as schematised in Figure 4.1b. The same evaluation was performed.

Once more, the behaviour of the exposure dose rate was analysed with increasing distance: at 1 m (P14, P16), at 2 m (P15) and at 3 m (P17). The horizontal angular influence was established at 0^o (P14, P15, P16) and at 120^o (P16). Finally, the vertical angular influence was assessed by placing the dosimeter at 0^o or 0 m height (P14), at 46^o or 1 m height (P18) and at 56^o or 1,5 m height (P19).

After each five minute point measurement, the data was exported to the PC and the values analysed as follows. Only values associated to a data acquisition error equal or below 5% were considered.

First, with the purpose of calculating the exact activity at the time of the measurement, $A(t)$, the time elapsed between $t = 0$ (time when the initial activity, $A(0)$, was registered) and the actual time of the measurement, was calculated. Then, following the fundamental decay equation (Equation 1.2), $A(t)$ was obtained. After subtracting the background dose rate to the dose rate measured, Γ was calculated in accordance to Equation 4.3, with being $(\mu Sv\ m^2)/(MBq\ h)$ the final units.

It was expected that despite variation of the measurement conditions, the ERC value remained, as the name implies, constant. However, that was not the case as it will be discussed thoroughly.

The purpose of this study is related to the fact that the assessment that will be conducted in the room intended for iodine radiotherapy will imply acquisition of exposure dose rates in strategic points arranged in different spatial locations. Moreover, the dosimeter will be placed immediately before and after the barrier. Therefore, it was crucial to determine the radiation behaviour in an open space without interference of close barriers to support the evaluation within the room.

Horizontal angular influence

Acquisition of all the points from P1 to P9 was only performed for ^{99m}Tc, since, as one can see by looking at Figure F.1A, the variation of the horizontal angle while keeping the distance to the source, does not seem to alter significantly the final ERC value, which corroborates the principle of isotropic source (see Section 3.6.1). Simultaneously, when the measurement is conducted at the floor level, the same behaviour was verified. Thus, from now on, let consider the average $\pm$ standard deviation of the separate measurements at the same distance to the source, as follows: $\overline{\text{P1}} = \overline{(\text{P1, P4, P7})}$; $\overline{\text{P2}} = \overline{(\text{P2, P5, P8})}$; $\overline{\text{P3}} = \overline{(\text{P3, P6, P9})}$; and $\overline{\text{P14}} = \overline{(\text{P14, P16})}$. The results are presented in Table 4.4. The horizontal angular influence was not assessed for the rest of the radionuclides since one just assumed that the same behaviour was transversal to all the radioactive species.

Table 4.4: ERC average value $\pm$ standard deviation (SD) for ^{99m}Tc concerning an isotropic source.

	Γ (μSv m^2)/(MBq h)	$\pm$SD
$\overline{\text{P1}}$	0,021166	0,000582
$\overline{\text{P2}}$	0,025577	0,000516
$\overline{\text{P3}}$	0,027972	0,001042
$\overline{\text{P14}}$	0,020389	0,000184

However, when comparing Figure F.1A and F.1B, one can conclude that when the measurements are performed on the floor, the value for ERC is slightly lower. This may be justified by the fact that only half of the air volume is available for the radiation to travel.

Distance influence

In this procedure the dosimeter and the radioisotope were at the same height. Through analysis of Figure F.2, one can see that globally, for all the radioactive species, the increasing distance results in an increasing ERC. When higher energies are involved, the rise with distance is more noticeable. Again, when on the floor, the ERC is lower than when at 1 m height, as well as the augmentation.

This behaviour is shown through the correlation functions of Table 4.5. One can observe that, for the same radioactive source, the ratio between the powers at z=0 over z=1 is approximately 0,5 which corroborates the assumption that at the floor level, the source is no longer considered

isotropic since only half of the air volume is available for the radiation to propagate.

Table 4.5: Correlation functions, y(d)=ad^b, illustrating the behaviour of Γ in (μSv m^2)/(MBq h) with distance d in m, for ^{99m}Tc, ^{67}Ga and ^{131}I, at 1 m (z=1) and 0 m (z=0). R^2 is the correlation coefficient, obtained with Excel®.

	^{99m}Tc		^{67}Ga		^{131}I	
z (m)	y	R^2	y	R^2	y	R^2
1	$0,0212d^{0,2559}$	0,9971	$0,0311d^{0,1923}$	1	$0,0606d^{0,1893}$	0,9999
0	$0,0204d^{0,1044}$	1	$0,0294d^{0,0971}$	0,9981	$0,0590d^{0,0960}$	0,9997

Vertical angular influence

Figure F.3 shows how ERC varies with alteration on the vertical height of dosimeter. In Figure F.3a the radioactive source is placed 1 m while in Figure F.3b the source is placed on the floor. Once more, the greater the distance between the measurer and the source, that is, the greater the angular displacement, the higher is ERC. This trend is visible for all the radionuclides. However the correlation functions of Table 4.5 do not represent the best approximation for this situation, as it was expected. Even the best approximation has an associated correlation coefficient to some extent far from 1 (Table 4.6). This may be justified by the fact that different geometries are mixed in the analysis: 4π geometry when the measurement is performed away from the floor and 2π when on the floor; and due to differences in the sensibility of the dosimetry concerning a vertical plane. In the dosimeter specifications, only information about anisotropy in the horizontal plane is given (see Appendix E).

Table 4.6: Correlation functions, y(d)=ad^b, illustrating the behaviour of Γ in (μSv m^2)/(MBq h) with vertical distance d in m, when ^{99m}Tc, ^{67}Ga and ^{131}I are placed at 1 m (z=1) and 0 m (z=0). R^2 is the correlation coefficient, obtained with Excel®.

	^{99m}Tc		^{67}Ga		^{131}I	
z (m)	y	R^2	y	R^2	y	R^2
1	$0,0209d^{0,201}$	0,9271	$0,0308d^{0,0977}$	0,841	$0,0602d^{0,1496}$	0,9507
0	$0,0208d^{0,4056}$	0,9517	$0,03d^{0,3236}$	0,9405	$0,0597d^{0,2972}$	0,9676

Build-up effect

As was possible to notice throughout the previous figures, ERC values for measurements performed on the floor were systematically smaller than the ones performed at 1 m height, for the same distance. This can be more clearly noticed by looking at Figure F.4. As explained before, this may be due to the different geometry available to irradiate, which results in less direct radiation. Therefore, when the radioactive source is on the floor, ERC is lower.

As the patient will spend most of his/her time on the bed, at approximately 1 m from the floor and at the distance of 1 m from the closest wall, the ERC obtained from P1 was used as reference for comparison purposes. In the case of ^{99m}Tc the reference value was the averaged $\overline{P1}$. Table 4.7 shows a comparison between the experimental reference value and the one calculated according to Stabin and Michael, 2007 [68] method. Globally, the experimental value is slightly higher than the theoretical one, which is more evident for ^{67}Ga. Nonetheless, one can say that the values are in agreement.

Table 4.7: Comparison of the ERC calculated theoretically in this work to the value determined after measuring the dose rate at the distance of 1 m from the radioactive source.

	Exposure rate constant (μSv m^2)/(MBq h)			
Radionuclides	Theoretical	Experimental	±SD	Ratio
^{99m}Tc	0,020084	0,021166	0,000582	0,95
^{67}Ga	0,019949	0,031063	0,000007	0,64
^{131}I	0,055197	0,060654	0,000149	0,91

One can conclude that both ERC determined theoretically and experimentally are in agreement to those values found in literature. However, when altering the experimental conditions at which the exposure dose rate is acquired, the resultant ERC does not remain constant. It was noticed that ERC increases when the distance between the radioactive source and the dosimeter is raised. On the other hand, ERC decreases when the measurement is performed at the floor level.

Chapter 5

Characterisation of the Unit Structure

Throughout this section, the unit-subject of this study will be referred as room n^{o} 401 (R401), since it is the first room in the corridor located on the fourth floor. Considering that R401 is located one floor above the new-borns floor, it was hypothesised the usability of room n^{o} 501 (R501) for accommodating the iodinetherapy treatment. At first glance, this room represent a better option since it is not preceded by a floor occupied by a group of people highly sensible to radiation.

Provided these considerations, the proper characterisation was conducted for both rooms following the exact same procedure, since, despite minor differences, both rooms presented the same geometrical arrangement.

The aim of this stage is to determine the physical characteristics of the construction materials present in the room structure. Each wall (floor and ceiling included), with thickness x, may be formed by one unique material (homogeneous material) or by a set of different materials (the most probable). As already explained (see Section 3.1.2), photon interactions with the absorbing media depend on the characteristics thereof, but also on the photons' energy, $h\nu$.

When traversing a material, the photon beam intensity is decreased depending on the material's thickness x and on the linear attenuation coefficient μ for a certain photon energy, according to Equation 3.10. For this reason, this procedure was conducted with recourse to three gamma-ray emitting radionuclides: ^{99m}Tc; ^{67}Ga; and ^{131}I, with distinct ranges of energy emission (Table 5.1). The linear attenuation coefficient considered for each radioactive source mentioned is in fact resulting from a weighted average concerning the yields at which the different energy amounts are emitted. Therefore, at this point, there are four variables for each wall:

- thickness (x);
- weighted average linear attenuation coefficient to ^{99m}Tc ($\overline{\mu}_{^{99m}Tc}$);
- weighted average linear attenuation coefficient to ^{67}Ga ($\overline{\mu}_{^{67}Ga}$); and
- weighted average linear attenuation coefficient to ^{131}I ($\overline{\mu}_{^{131}I}$).

Table 5.1: Most significant energy spectra for ^{99m}Tc, ^{67}Ga and ^{131}I (adapted from NuDat 2.6 [70, 71, 72]).

Radioisotope	Energy (keV)	Yield
^{99m}Tc	140,511	0,89
^{67}Ga	93,310	0,39
	184,576	0,21
	300,217	0,17
	393,527	0,05
^{131}I	284,305	0,06
	364,489	0,82
	636,989	0,07
	722,911	0,02

A round of measurements was performed for each of these radionuclides. In each round, the exposure dose rates were measured when the radioisotopes were placed at two distinct strategic points, at a known distance from the walls:

- Bed — where the patient will spend most of her/his time; and
- Toilet — where the patient will spend a considerably amount of time.

In each measurement of each round, after placement of the radionuclide in one of the strategic points, a dosimeter (AT1121, Atomtex®- see Appendix E for detailed specifications) was placed immediately before and after the shielding barrier at distinct times, as schematised in Figure 5.1.

The attenuation provided by the barrier with thickness x, to a given radiation energy, was calculated according to Equation 3.11, after measuring the exposure dose rate before ($\delta D_i/\delta T$) and after ($\delta D_f/\delta T$) the attenuation. Only values associated with an error less or equal to 5% were considered in the average exposure dose rate calculation.

The calculated thickness does not correspond to the exact dimension of the barrier but to the lead-equivalent thickness (in millimetres of lead, mmPb). That is, it was determined which thickness of lead would provide the same attenuation to a given amount of energy as the heterogeneous wall provides. The lead mass attenuation coefficients (μ_m) for the radionuclides' energies were obtained by interpolation of Hubbell and Seltzer, 1996 [65] data. Given that the lead density is 11,350 g cm^{-3}, the linear attenuation coefficients (μ) were easily obtained. The points of interest were distributed in the room in accordance to Figure 5.2. They were chosen based on the occupancy factor and the operational actions developed in the surrounding areas. All points are marked at 1 m from the floor, simulating the level at the patient bed, despite points F and G that represent the ceiling and the floor, respectively, and O2 that represent the toilet.

All the measurements were conducted in R401 and R501. The only difference between the rooms is that point C does not exist in R501. Since point C corresponds to a door, in R401 the

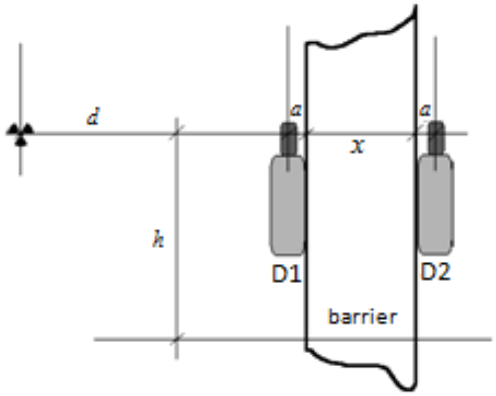

Figure 5.1: Diagram for the measurement of the exposure dose rate, where: d is the distance between the radioactive source and the interior limit of the barrier, where one detector (D1) is located; a is the distance between the detector and the limit of the barrier (although it was neglected since it represents a small distance when compared to d); x is the thickness of the barrier; h is the distance between the floor and the detectors level. D2 is located in the exterior limit of the barrier, at the same distance h from the floor as D1.

exposure dose rate before and after point E was measured twice, with that door closed (Ec@O1) and opened (Eo@O1).

Electromagnetic radiation travels in a straight line, so equally important to the placement of the strategic points is the distance between each one of them and the radioactive source of energy, which is present in Table 5.2. This distance is represent in Figure 5.1 by d.

Table 5.2: Coordinates of all points of interest in R401, when the referential origin is placed at O1 from Figure 5.2, and straight-line distances, d, from O1 and O2 to the points where the measurements were held. All the distances are in cm.

Radioactive source	Measurement point	x	y	z	d
	A	0	100	100	100
	B	-200	-70	100	211,90
	C	-200	-170	100	262,49
O1	D	200	-321	100	378,21
	E	-437	-179	100	472,24
	F	0	0	270	170
	G	0	0	0	100
O2	D	200	-321	100	122,07

After obtaining the initial activities in Instituto CUF, the radionuclides were transferred to Hospital CUF where the characterisation of the unit was performed. The activities at the start of the measurement are shown in Table D.2. Again, this was validated in Section 4.1.

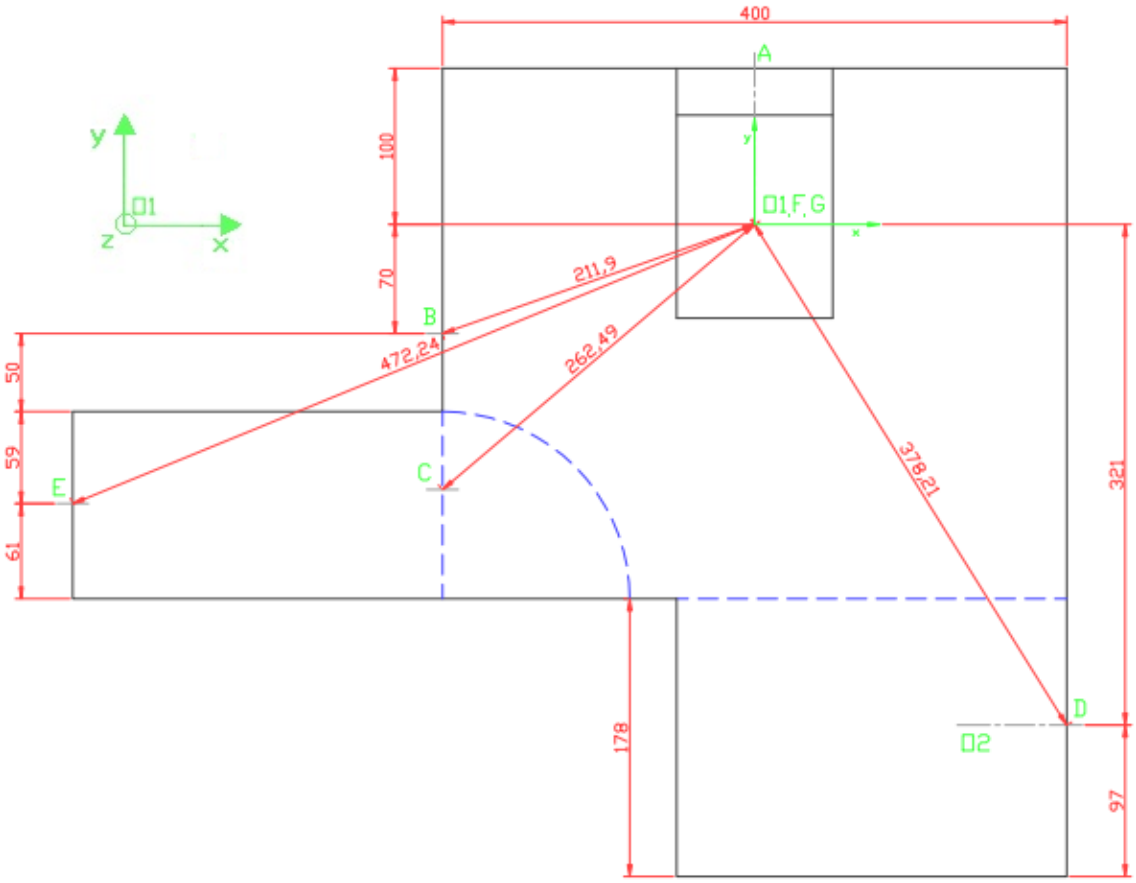

Figure 5.2: Layout of the R401 therapy room with the marked points of interest: A — contact point with another unit; B — contact point with machinery room; C — door that separates the room itself from the hall that gives access to the room; D — bathroom and contact point with another unit; E — entrance/exit door that separates the unit hall from the corridor, where other patients, exposed workers and members of the public are with very high frequency; F — ceiling and contact point with another unit in the floor immediately above; G — floor and contact point with another unit in the floor immediately below; O1 — first reference point, located in the bed; O2 — second reference point, located in the toilet. The distances are in cm.

The calculated weighted average linear attenuation coefficients for the three radionuclides are presented in Table 5.3. The weighted average is used, instead of considering the attenuation only to the higher energy, which for these radioisotopes are emitted with the least yields, in order to avoid oversizing of the existent barrier. As one can see, the overall increase in the γ energy emission results is a lower attenuation per centimetre of lead (cmPb), meaning that fewer photons are removed from the incident beam.

After calculation of μx by applying Equation 3.11, such that:

$$\overline{\mu}x \quad = \quad -\ln(\delta D_f/\delta D_i), \tag{5.1}$$

for each radioisotope, at each strategic point, the estimation of lead-equivalent thickness (x) was

Table 5.3: Weighted average linear attenuation coefficients (cm^{-1}) for lead, concerning the weighted average gamma energy (keV) emitted during decay.

	$\overline{E}$ (keV)	$\overline{\mu}$ (cm^{-1})
^{99m}Tc	140,511	30,473
^{67}Ga	176,409	29,360
^{131}I	386,185	3,285

straightforward. The results are present in Table 5.4 and Table 5.5, for R401 and R501, respectively. The first thing that is noticed is that clearly the attenuation phenomenon strongly depends on the photons energy.

Table 5.4: Lead-equivalent thickness (mmPb) in R401.

	^{99m}Tc		^{67}Ga		^{131}I	
R401	μx	x (mmPb)	μx	x (mmPb)	μx	x (mmPb)
A@O1	5,64	1,85	2,16	0,73	1,33	4,04
B@O1	4,60	1,51	2,12	0,72	1,77	5,39
C@O1	4,15	1,36	1,65	0,56	1,02	3,11
D@O1	1,65	0,54	1,64	0,56	2,22	6,75
D@O2	5,40	1,77	2,62	0,89	1,73	5,26
Ec@O1	0,15	0,05	0,06	0,02	0,20	0,61
Eo@O1	0,30	0,10	0,12	0,04	0,28	0,85

Firstly, let one look at the behaviour of μx. As it is a negative logarithmic function (Equation 5.1), the lower $\delta D_f/\delta D_i$, the higher the resulting μx. As $\delta D_f/\delta D_i$ represents the ratio between the dose after and before the barrier, smaller ratios are indicators of greater attenuation. In the limit, there is no attenuation. Thus, D_f tends to equal D_i and the ratio tends to 1 and μx to 0. Table 5.4 reflects this trend. In a general way, μx is systematically higher as the energy of the radioactive source decreases (from ^{131}I to ^{99m}Tc), meaning that for lower energies the attenuation is higher.

As the measurement points were chosen to be distributed along barriers edified with different purposes, it was not expected they would attenuate the radiation in the same manner. However, there is one exception: D@O1 and D@O2 refer to the same barrier, and for this reason the theoretical attenuation should have been the same, which was not verified. The difference between both experiments is only the source placement: O1 at 1 m from the floor and O2 on the floor. As it was already discussed in Section 4.2, the alteration in the radiation field geometry seems to affect the exposure dose rate and consequently, the attenuation registered may not be representative.

Another unexpected outcome is related to point E. This barrier was subjected to two measurements: the first in the presence of barrier C (Ec@O1) and the second in its absence (Eo@O1). In the first situation, the energy is firstly attenuated by barrier C and then by barrier E; in the second, the radiation travels in a straight line until attenuated by E. It was verified that in the former the

exposure dose rate acquired at the interior limit of E was lower than in the latter (data not shown). Therefore, theoretically barrier E should provide the same attenuation.

Since ^{131}I is the radionuclide with wider range of energy emission, the lead-equivalent thickness is naturally higher than for the others radioactive sources used. Then, even for a lower attenuation, it is needed an absorber material with higher thickness than in the presence of lower energies.

Table 5.5: Lead-equivalent thickness (mmPb) in R501.

	^{67}Ga		^{131}I	
R501	μx	x (mmPb)	μx	x (mmPb)
A@O1	0,85	0,29	0,76	2,30
B@O1	0,75	0,25	0,70	2,14
D@O1	1,66	0,57	2,68	8,15
D@O2	3,54	1,20	3,01	9,16
Eo@O1	0,26	0,09	0,33	1,00

In R501, the same overall behaviour was verified (Table 5.5). In this room, the measurements were only performed with ^{67}Ga and ^{131}I due to the higher energies associated.

Exposure dose rates at F and G are not shown since the values were relatively small and for this reason neglected. The exposure dose rate at F was acquired when the radioactive source was placed at O1 and O2, in order to quantify the attenuation provided by the ceiling. Due to the small magnitude of the values, one just concluded that the ceiling provided the desired attenuation. This assumption can also be applied to the floor, since they are both constituted by the same materials.

This experiment allowed concluding about the existent barriers of rooms 401 and 501 in lead-equivalent thickness (mmPb). When comparing the results for both rooms, it is legitimate to admit that the attenuation provided by the construction materials of R401 is higher which could mean that some amount of shielding material was actually incorporated in the unit design.

Nonetheless, despite the attenuation provided, it was confirmed that the exposure dose rate after the barriers was far from the regulatory values established by legislation, even in the presence of the lowest energies. According to D.L. n^{o}222/2008, on 17th July 2008 [63] the maximum dose limit for members of the public is 1 mSv/y, that is, 0,114 μSv/h.

Moreover, this experiment was conducted for small activities, while the radiotherapy may use activities of ^{131}I up to 200 mCi, which is twenty times higher, and according to Equation 3.8, the exposure dose rate is directly proportional to the activity. Therefore, the shielding barriers should be reinforced with an effective absorber material whose thickness was determined and explained in the next section.

Chapter 6

Shielding Plan

Standard therapy with ^{131}I is given as fixed activities. Small cancers confined to thyroid may receive the lowest dose (1110 MBq or 30 mCi) while more advanced cancers with metastases at distance receive higher doses (up to 7400 MBq or 200 mCi) [6, 26]. The retained activity, however, changes over time. This quantity depends on the administered activity, the mass and function of the thyroid tissue and the rate of clearance, that can be stimulated by patient's hydration and renal function [52].

Figure 6.1 shows a simulation of dose rate at 1 m and the radioiodine decay concerning the calculated effective half-life (T_e) of 7,52 days (Section 2.2.1.2) that takes into account both the physical ($t_{1/2}$) and the biological half-life (T_b). This simulation represents the worst case scenario since the rate of clearance is not considered. If it was, 24h after administration of radioiodine, the activity would probably correspond to 12–40% of initial value [47].

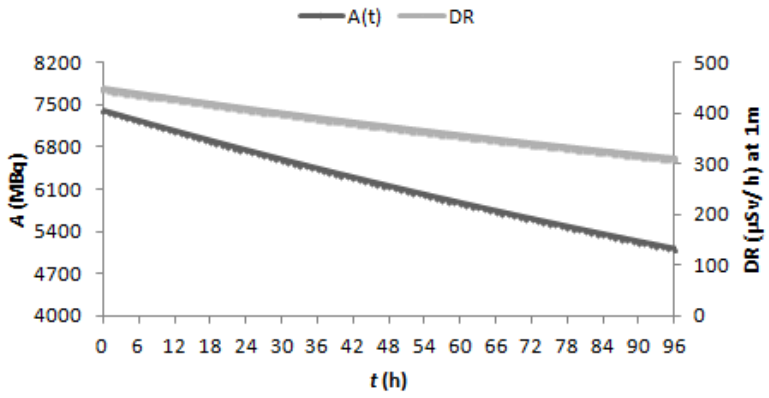

Figure 6.1: Simulation of the decay and expected dose rate (μSv/h at 1 m) for radioiodine with initial activity of 7400 MBq (or 200 mCi), assuming a $T_e = 7,52$ days.

After radioactive iodine (RAI) administration, the patient is kept in an isolated unit with a single-bed with dedicated toilet and ablution facilities, until the radiation dose rate drops below 30 μSv/h [60]. This amount is strongly influenced by thyroid mass, patient orientation and biodistribution of the radiopharmaceutical within the organism (see Figure 2.7) and should be measured

with a portable survey meter held at a distance of 1 m anterior to the patient's neck. This unit should be prepared to minimise the radiation exposure to acceptable values, and for this reason the shielding design should consider the extreme situation, that is, the highest dose administered and an occupancy factor of 1 in the vicinity of the premises (Table 3.1).

For that, the exposure to ^{131}I with activity of 7400 MBq (or 200 mCi) was simulated in the strategic points defined before (Figure 5.2). Equation 3.8 allows estimating the exposure dose rate that should be expected. Γ was calculated on the basis of the assumptions concluded from the experiments performed before.

Thus, in the calculation of the exposure rate constant for the points measured when the radioactive source is at 1 m height from the floor (z=1), i.e., simulating the patient lying on the bed, the function from Table 4.5 was used. When the radiation source was place on the floor (z=0), simulating the patient in the toilet, the function from Table 4.6 was applied. The distance d represents the straight line distance between the radiation source and the each point, which are present in Table 5.2. By knowing Γ, the expected exposure dose rate for each point was determined following Equation 3.8. Considering the dose limit of 0,114 μSv/h as the maximum exposure dose rate after the barriers, the necessary lead-equivalent thickness was determined by application of Equation 5.1. The linear attenuation coefficient considered is present in Table 5.3. After knowing the necessary thickness to attenuate the radiation in that extent, the existent thickness was subtracted and the reinforcement determined.

The expected dose rate determined for ^{131}I with initial activity of 7400 MBq (or 200 mCi) at the strategic points is shown in Table 6.1. As one can see, the exposure rate within the unit will be extremely high. Thus, in order to minimise the exposure on the outer side of the barriers to the maximum value of 0,114 μSv/h, a considerable amount of attenuation should be implemented. This amount is quantified in Table 6.2 by means of μx.

Table 6.1: Expected exposure dose rate, at the interior limits of the barrier (indicated by i), for ^{131}I with initial activity of 7400 MBq or 200 mCi.

Points	Γ (μSv m^2)/(MBq h)	$\delta D_i/\delta T$ (μSv/h)
A_i@O1	0,060600	448,44
B_i@O1	0,069857	115,13
C_i@O1	0,072746	78,13
D_i@O1	0,077954	40,33
D_i@O2	0,063345	314,60
Ec_i@O1	0,081300	26,98
Eo_i@O1	0,081300	26,98

Lead (Pb) was the chosen shielding material since it possesses highly desirable properties, such as high density ($\rho = 13,350$ g cm^{-3}) and high atomic number ($Z = 82$). The high density provides

Table 6.2: Lead-equivalent thickness (mmPb) necessary reinforcement for ^{131}I with initial activity of 7400 MBq or 200 mCi.

			R401		R501	
Points	μx	x total (mmPb)	mmPb existent	mmPb needed	mmPb existent	mmPb needed
A@O1	8,28	25,20	4,04	21,16	2,30	22,90
B@O1	6,92	21,06	5,39	15,67	2,14	18,92
C@O1	6,53	19,88	3,11	16,77		
D@O1	5,87	17,87	6,75	11,11	8,15	9,72
D@O2	7,92	24,12	5,26	18,86	9,16	14,96
Ec@O1	5,47	16,64	0,61	16,03		
Eo@O1	5,47	16,64	0,85	15,80	1,00	15,65

greater attenuation for a given thickness, while the large Z number increases the probability of an interaction to occur. The more interactions take place, the greater is the attenuation. The most probable interactions' types are present in Section 3.1.2.

The lead thicknesses necessary to provide the desired attenuation are present in Table 6.2. Although a more close observation indicates that the barriers A, B (mostly in R401) and D (mostly in R501) already present some amount of shielding material, an overall look indicates that the adequate reinforcement approximates 2 cmPb (1,65 $\pm$ 0,37 cmPb) for all the chosen points.

Lead is effective in shielding gamma radiation, while for β particles a first layer of a material with smaller Z is more indicated. This double-layered shield aims to attenuate high-energy beta radiation while minimising bremsstrahlung [2, 44]. In this work, the first layer was not taken into account since the charged particles emitted during decay of ^{131}I are practically restricted to the thyroid gland and hence, will hardly reach the shielding walls due to the weak penetrating power.

Chapter 7

Conclusion

Radioiodine therapy is subjected to strict regulatory control that seeks to provide safety to others than the patients submitted to the radiotherapy for thyroid cancer treatment. Whenever the patient is administered with iodine with activity higher than 740 MBq (or 20 mCi), he/she should be kept in an isolation unit until the radiation exposure dose rate, measured at 1m anterior to the patient's neck, drops below 30 μSv/h.

According to D.L. n^{o}222/2008, on 17th July 2008 [63], the maximum exposure dose limit for members of the public is 1 mSv/y, that is, 0,114 μSv/h. Therefore, the walls of the facility should strongly attenuate the radiation emitted by the radioisotope inside the room, so outside the room the exposure is always bellow the accepted limit, even for the extreme situations that assume an initial activity of 200 mCi and an occupancy factor of 1.

The present work allowed to conclude that the current dimensions and materials that constitutes the unit walls do not efficiently attenuate the emitted γ radiation. This experiment was conducted for different radioactive sources with different range of energy emission (from 93–723 keV). Thus, it is proposed a shielding plan that suggests a reinforcement of the walls with at least 2 centimetres of lead (cmPb) to the already existing materials. The determination was based on the assumption that, in practice, the exposure rate constant in air is influenced by the distance between the radioactive source and the absorber material.

Following the proposed solution, the patient will benefit from the radioactive treatment while in the surrounding areas of the therapeutic room the exposure will be kept as minimal as possible and legally accepted concerning the dose limit established for members of the public.

As future work, the shielding barriers could be weight, volume and cost optimised. Although β particles have weak penetration power and probably would not reach the wall when the patient is placed at bed, a first layer of a material with smaller Z, such as plastic or glass, could also be added to the shielding barrier. This double-layer would attenuate β particles while minimising bremsstrahlung, providing an efficient shield in case the patient leans against the wall. The room design, structure and operational management could also be improved so it gathers the adequate conditions for the number of treatments to be performed, the flow of patients and decontamination purposes between patients.

Appendix A

Decay Schemes

^{131}I decays into ^{131}Xe (Xenon) with a half-life of 8,0233 days by emission of β minus followed by γ radiation. The primary emissions are electrons with energies between 248 keV and 807 keV, but 89% is 606 keV, followed by photon emission with energies between 80 keV and 723 keV, with 81% abundance of 364 keV.

^{99m}Tc is a metastable nuclear isomer. This term, denoted by the letter "m" after the mass number, is an indication that its nucleus stays in an excited state longer than $10^{-}12$ seconds [2]. The nucleus will eventually relax to its ground state by γ emission of 141 keV with a yield of 89%, which only rearranges the nucleons. ^{99m}Tc half-life ($t_{1/2}$) is 6,0067 hours.

^{67}Ga has a $t_{1/2}$ of 3,2613 days. It decays into ^{67}Zn (Zinc) by electron capture followed by gamma emission with energies between 93 keV and 888 keV.

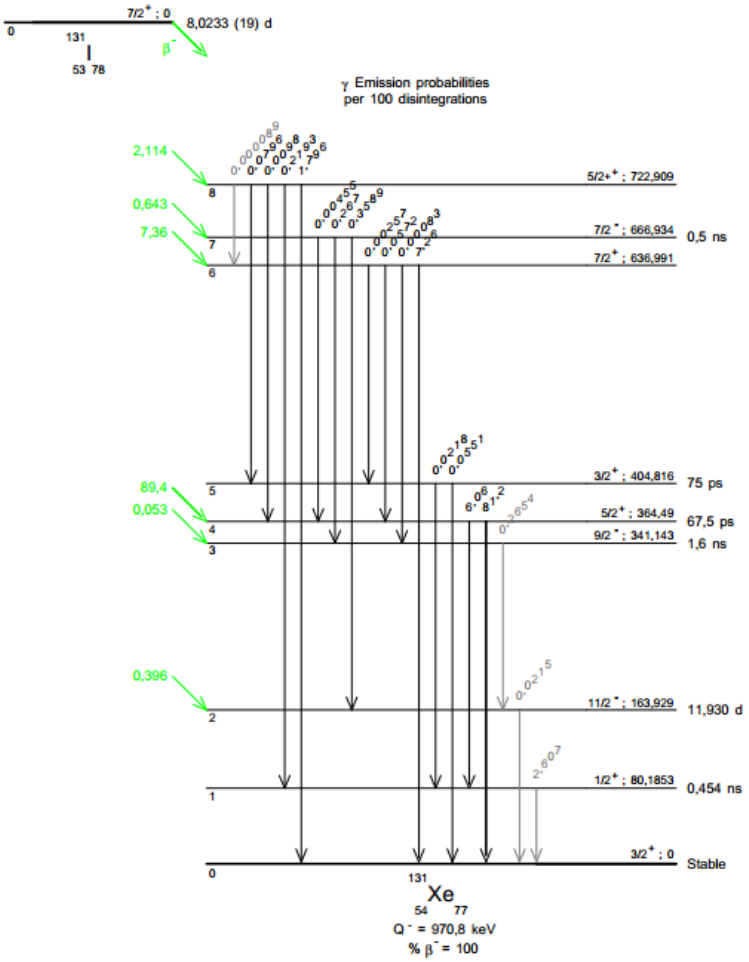

Figure A.1: Decay scheme of Iodine-131 (^{131}I) [43].

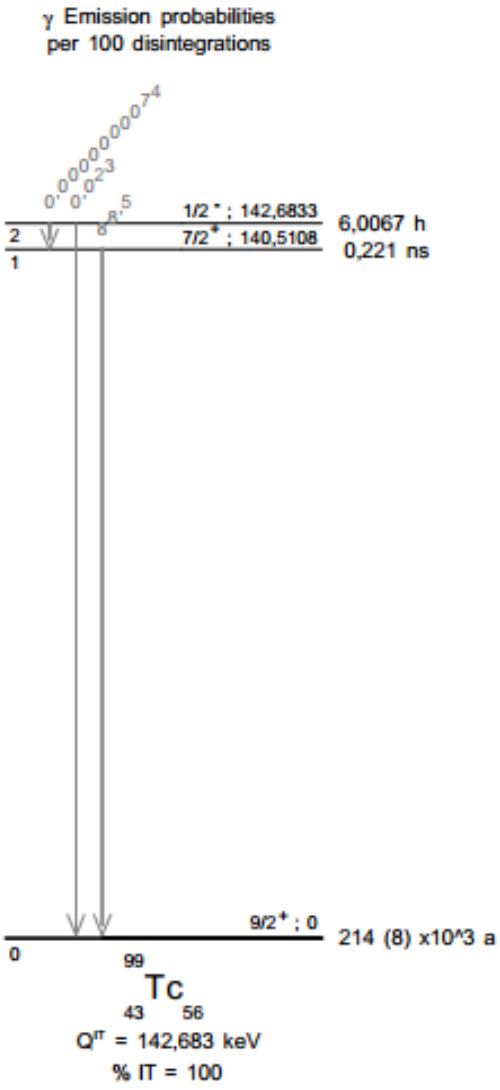

Figure A.2: Decay scheme of Technetium-99m (^{99m}Tc) [43].

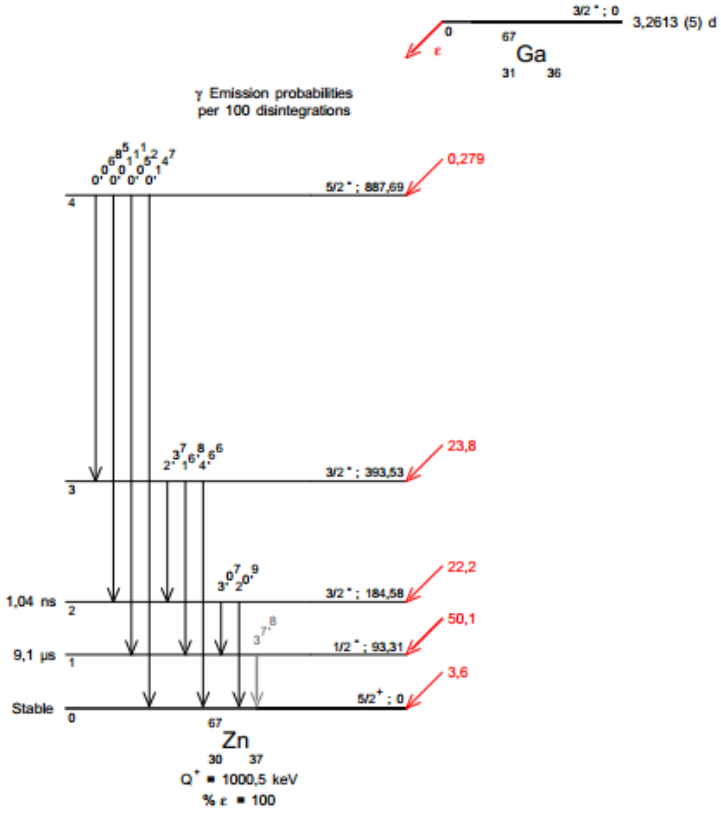

Figure A.3: Decay scheme of Gallium-67 (^{67}Ga) [43].

Appendix B

Weighing Factors

Tissue weighing factor, w_T, for different tissues and organs and radiation weighing factor, w_R, for different radiation types according to Directive L 013, OJEU, on 17th January 2014 [4]. w_T for thyroid gland is 0,04. For photons (γ) and electrons (β^-) emission, w_R equals 1.

Table B.1: Tissue weighing factor, w_T, for different tissues and organs (from [4]).

w_T	Tissue or organ
0,12	Breast, Bone-marrow (red), Colon, Lung, Stomach
0,08	Gonads
0,05	Remainder tissues
0,04	Bladder, Liver, Oesophagus, Thyroid
0,01	Bone surface, Brain, Salivary glands, Skin

Table B.2: Radiation weighing factor, w_R, for different radiation types (from [4]).

w_R	Radiation type
1	Photons, Electrons
2	Protons
5–20	Neutrons
20	Alpha

Appendix C

Experimental Decay Values

Logarithmic representation of the fundamental decay equation (Equation 1.2), where $A(0)$ represents the initial activity, at time $t = 0$, $A(t)$ the measured activity at the time t the values were registered (shown in the tables) and λ the decay constant, for ^{99m}Tc, ^{67}Ga and ^{131}I. The slope of each graph represents the decay constant. For each radioisotope, the experimental λ is the average of the decay constants obtained from the measurements performed with the two dose calibrators followed by application of appropriate unit conversions. The respective half-life ($t_{1/2}$) was obtained after application of Equation 1.3.

Table C.1: Experimental values of ^{99m}Tc activity (in mCi) at different times (t), demonstrating an exponential decay. Activity values shown result from the average values measured with two different dose calibrators.

t	$A(t)$ (mCi)
00:00:00	3,5017
00:33:16	3,2771
01:16:15	3,0207
01:51:54	2,8242
02:31:14	2,6117
02:57:10	2,4899
03:49:51	2,2436
04:39:29	2,0412
05:20:17	1,8865

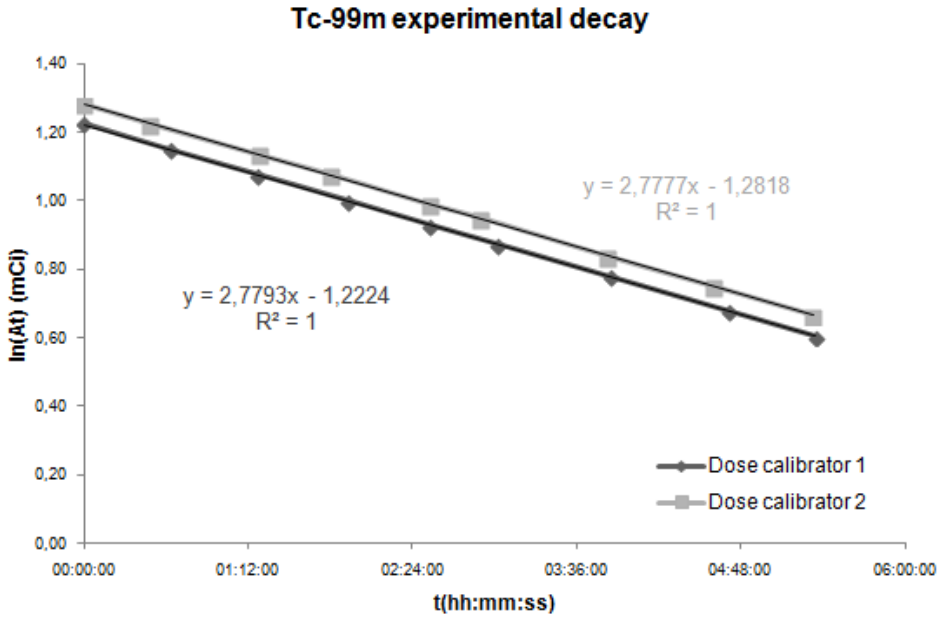

Figure C.1: Logarithmic representation of ^{99m}Tc measured activity ($A(t)$) in mCi vs. time (t).

Table C.2: Experimental values of ^{67}Ga activity (in mCi) at different times (t), demonstrating an exponential decay. Activity values shown result from the average values measured with two different dose calibrators.

t	$A(t)$ (mCi)
0:00:00	0,3325
4:45:00	0,3168
23:37:00	0,2713
28:44:00	0,2561
53:19:00	0,2077
124:49:00	0,1164
196:49:00	0,0593
221:04:00	0,0478

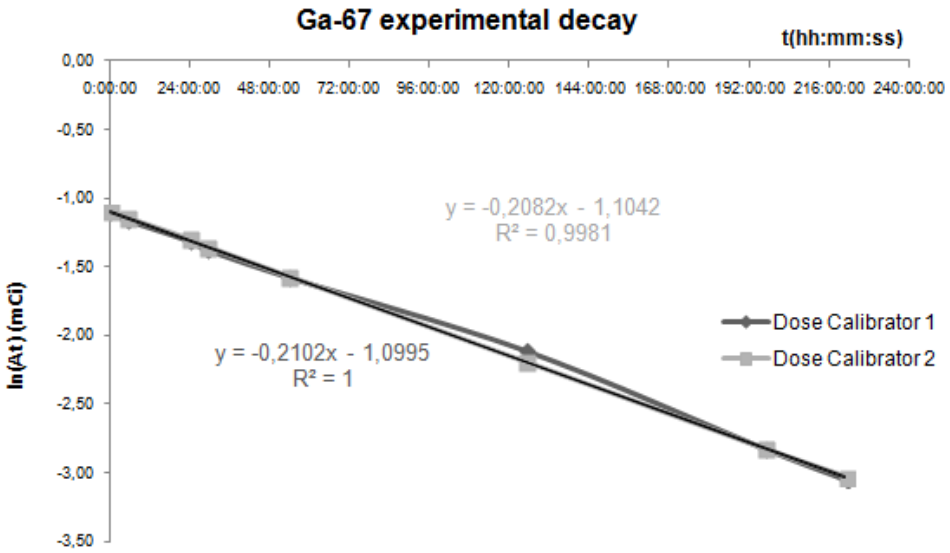

Figure C.2: Logarithmic representation of ^{67}Ga measured activity ($A(t)$) in mCi vs. time (t).

Table C.3: Experimental values of ^{131}I activity (in mCi) at different times (t), demonstrating an exponential decay. Activity values shown result from the average values measured with two different dose calibrators.

t	$A(t)$ (mCi)
0:00:00	0,6651
22:35:00	0,6263
46:33:00	0,5734
71:00:00	0,5283
94:30:00	0,4854
115:05:00	0,4526
166:30:00	0,3787
190:30:00	0,3484

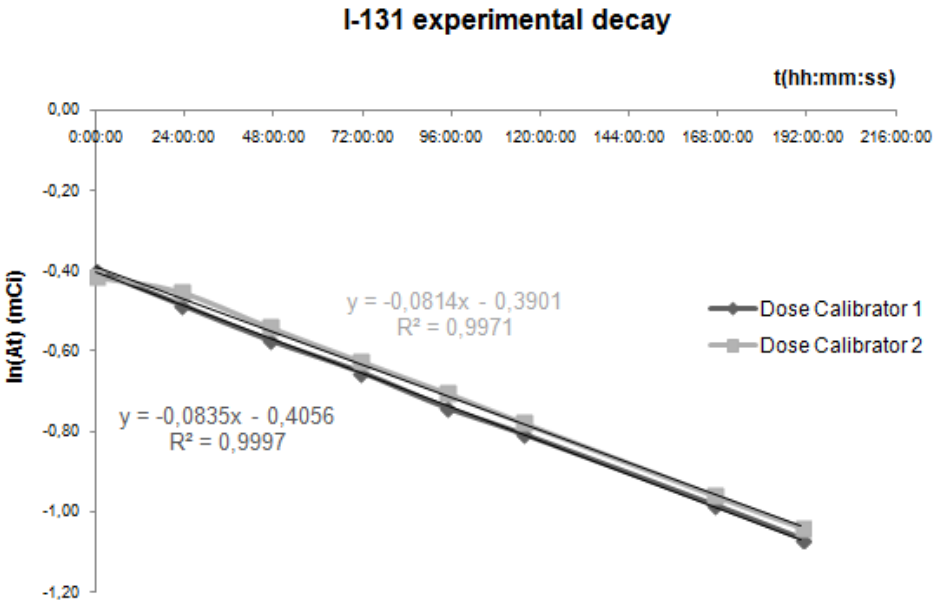

Figure C.3: Logarithmic representation of ^{131}I measured activity ($A(t)$) in mCi vs. time (t).

Appendix D

Initial Activities

Initial activities ($A(0)$) for each radioisotope for the exposure rate constant (ERC) determination and the unit characterisation.

Table D.1: Initial activity for each radioisotope for ERC determination.

	Initial activity $A(0)$	
Radioisotope	mCi	MBq
^{99m}Tc	21,88	809,56
^{67}Ga	8,17	302,29
^{131}I	13,72	507,64

Table D.2: Activity at the start of the measurement for the characterisation experiment.

	Initial activity $A(0)$	
Radioisotope	mCi	MBq
^{99m}Tc	59,42	2198,54
^{67}Ga	8,54	315,98
^{131}I	13,87	513,19

Appendix E

Dosimeter Specifications

The acquisition of the exposure dose rates was performed using a portable dosimeter (Atomtex®, model AT1121) able to detect photon radiation from 15 keV to 10 MeV and dose rate from 50 nSv/h to 10 Sv/h. The overall dimensions of AT1121 are $233 \times 85 \times 67$ mm with a weight of 0,9 kg. The device detector is made of a scintillation plastic with a diameter of 30 mm and a length of 15 mm. The portable dosimeter is presented in Figure E.1.

Figure E.1: Portable dosimeter from Atomtex®, model AT1121.

The dosimeter was set to acquire the dose rate every second, which was automatically shown in the LCD screen thereof. AT1121 also registered the date and time of each measurement, the associated error and the maximum dose rate for the time of the experiment. Only values associated to an error equal or below 5% were considered in the posterior calculations. The intrinsic relative measurement error is $\pm 15\%$.

The sensitivity of the dosimeter is influenced by the radiation source position and energy emission concerning the horizontal plane around the dosimeter, according to Figure E.2. The

accuracy is maximal when the dosimeter detector is facing the source. No information concerning anisotropy in the vertical plane was provided by the supplier in the specification sheet [76].

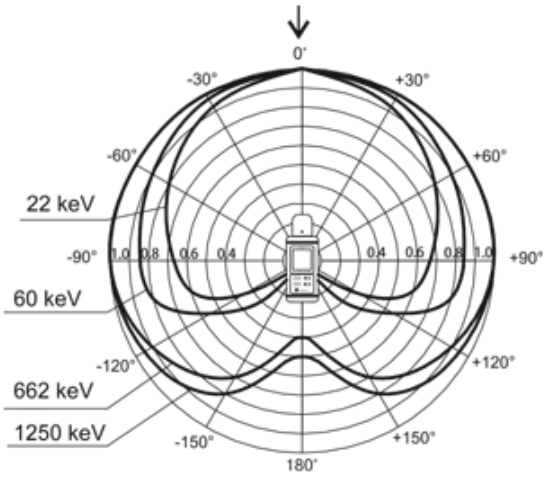

Figure E.2: Standard dosimeter anisotropy for horizontal plane (adapted from [76]).

The dosimeter was manipulated through the PC, by Mediana software from the same supplier. After each acquisition, the data was stored in the PC in a text document, from which the results were extracted to be analysed with Excel®.

Appendix F

Experimental Exposure Rate Constant Values

Study of the influence of the distance between the dosimeter and the radiation source on the exposure rate constant (ERC or Γ) value for ^{99m}Tc,^{67}Ga and ^{131}I.

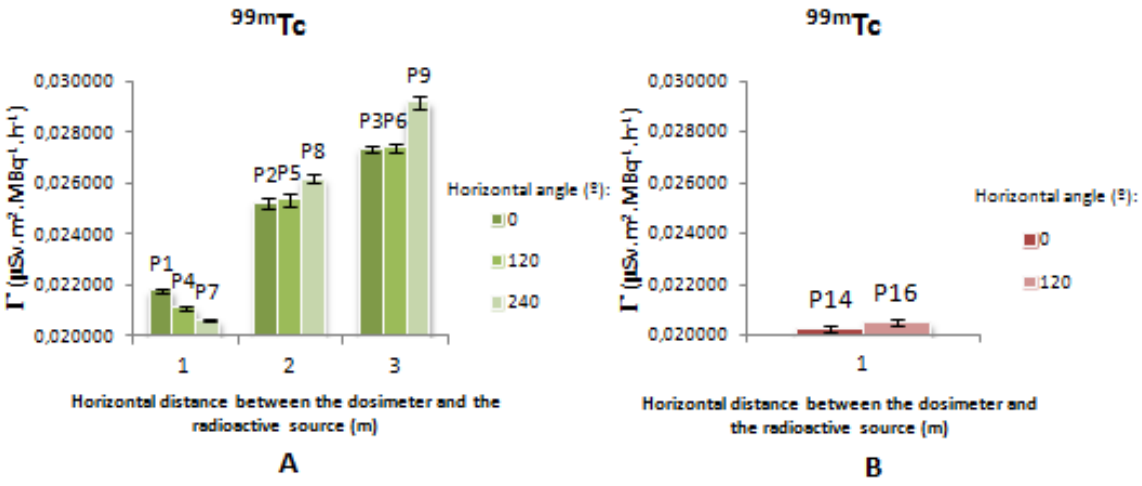

Figure F.1: Horizontal angular influence at A) 1 m and B) 0m height for ^{99m}Tc.

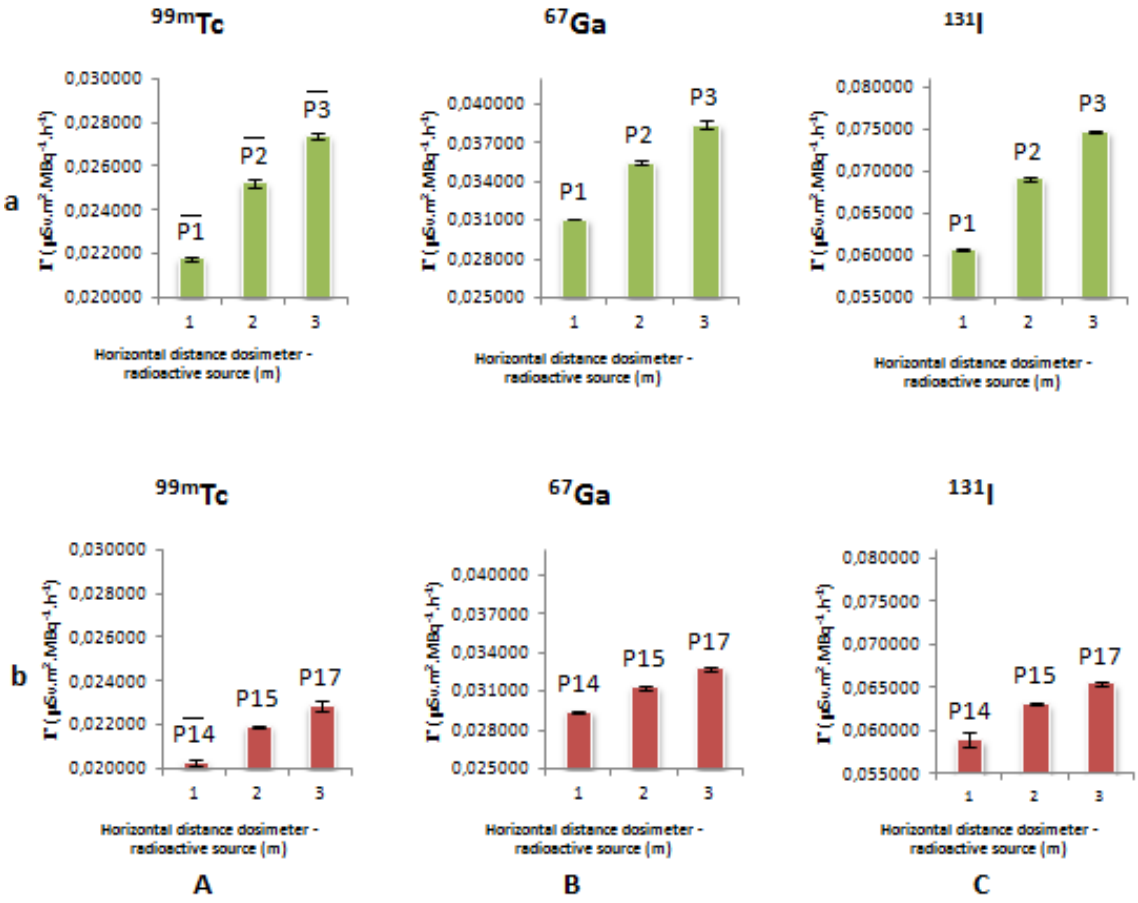

Figure F.2: Influence of the increasing distance in the ERC value at a) 1 m and b) 0 m for A) ^{99m}Tc, B) ^{67}Ga and C) ^{131}I.

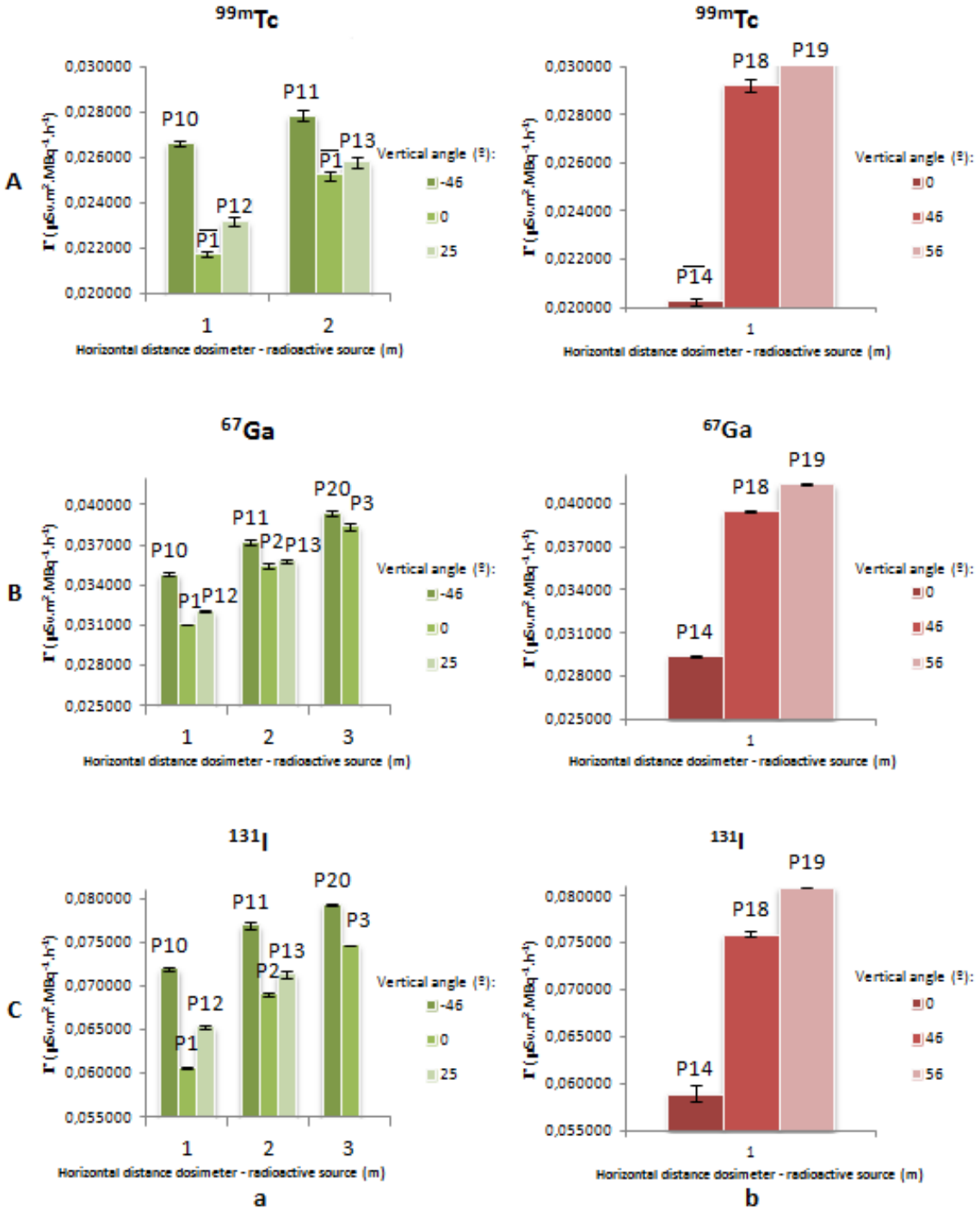

Figure F.3: Influence of the angular displacement in vertical direction when the radioactive source is placed at a) 1 m and b) 0 m height for A) ^{99m}Tc, B) ^{67}Ga and C) ^{131}I.

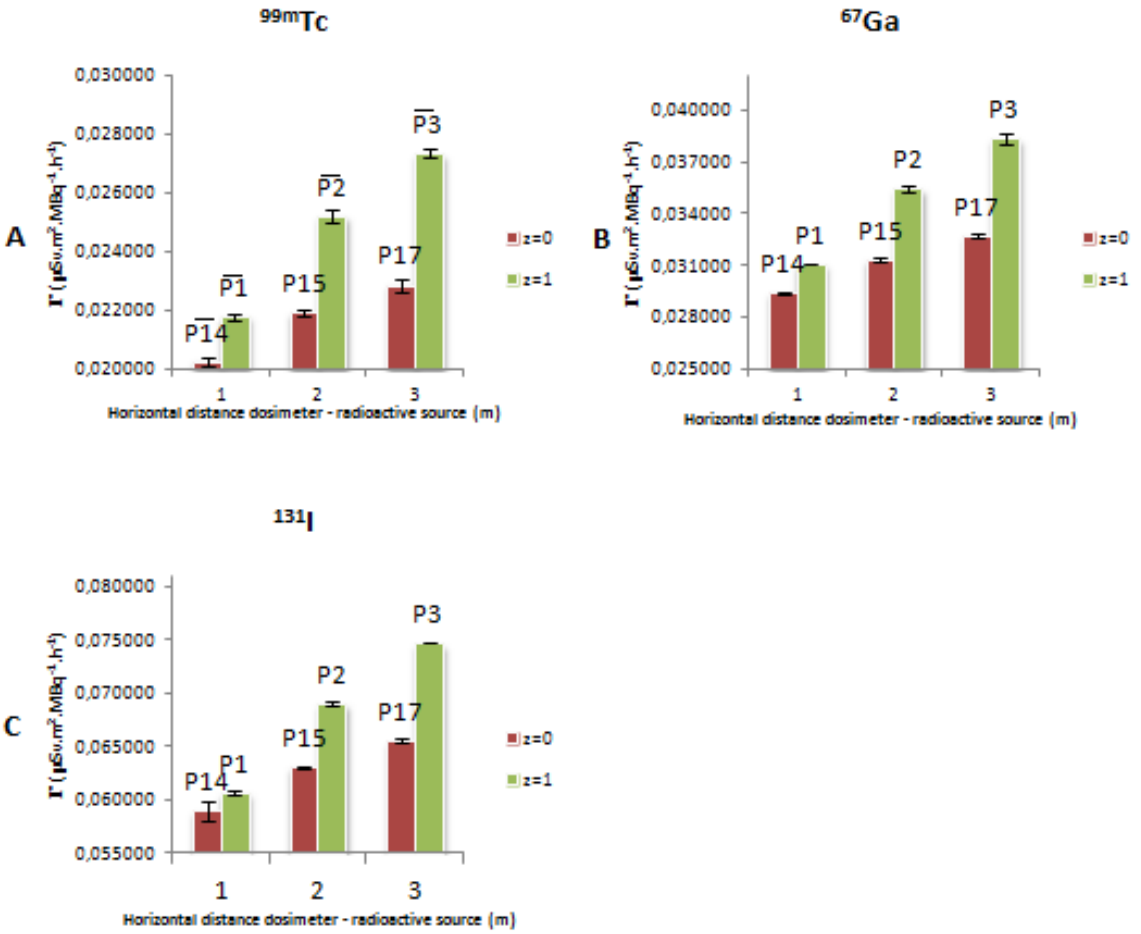

Figure F.4: Comparison of ERC measured at 1 m and 0 m height for A) ^{99m}Tc, B) ^{67}Ga and C) ^{131}I.

References

[1] Marcelo Tatit Sapienza, Irene Shimura Endo, Guilherme C. Campos Neto, Marcia G.M. Tavares, and MarÃlia M.S. Marone. Tratamento do carcinoma diferenciado da tiroide com iodo-131: intervenção para aumentar a dose absorvida de radiação. *Arquivos Brasileiros de Endocrinologia & Metabologia*, 49:341 – 349, 06 2005.

[2] Jerrold T Bushberg and John M Boone. *The essential physics of medical imaging*. Lippincott Williams & Wilkins, 2011.

[3] Ervin B Podgorsak. *Radiation physics for medical physicists*. Springer, 2010.

[4] European Union. Official Journal of the European Union, L 013, 2014.

[5] Group Diagram. *Chemistry: An Illustrated Guide to Science*. Infobase Publishing, 2006.

[6] Furio Pacini, Martin Schlumberger, Henning Dralle, Rossella Elisei, Johannes WA Smit, Wilmar Wiersinga, et al. European consensus for the management of patients with differentiated thyroid carcinoma of the follicular epithelium. *European journal of endocrinology*, 154(6):787–803, 2006.

[7] J Ferlay, E Steliarova-Foucher, J Lortet-Tieulent, S Rosso, JWW Coebergh, H Comber, D Forman, and F Bray. Cancer incidence and mortality patterns in Europe: estimates for 40 countries in 2012. *European Journal of Cancer*, 2013.

[8] EUCAN. Country Factsheets, 2013. http://eco.iarc.fr/eucan/Country.aspx?ISOCountryCd=968.

[9] R Görges. The changing epidemiology of thyroid cancer. In *Thyroid cancer*, pages 3–27. Springer, 2005.

[10] Gabriella Pellegriti, Francesco Frasca, Concetto Regalbuto, Sebastiano Squatrito, and Riccardo Vigneri. Worldwide Increasing Incidence of Thyroid Cancer: Update on Epidemiology and Risk Factors. *Journal of cancer epidemiology*, 2013.

[11] Briseis Aschebrook-Kilfoy, Raymon Grogan, Mary Ward, Edwin Kaplan, and Susan Devesa. Follicular Thyroid Cancer Incidence Patterns in the United States, 1980-2009. *Thyroid*, 2013.

[12] Rebecca L Brown, Jonas A de Souza, and Ezra EW Cohen. Thyroid cancer: burden of illness and management of disease. *Journal of Cancer*, 2:193, 2011.

[13] ND Denise Kirsten. The Thyroid Gland: Physiology and Pathophysiology. *Thyroid*, 1(4):11, 2000.

[14] Rod R Seeley, Trent D Stephens, and Philip Tate. Anatomy and physiology. *New York, NY: McGraw Hill*, 2003.

[15] John E Hall. *Guyton and Hall Textbook of Medical Physiology: Enhanced E-book*. Elsevier Health Sciences, 2010.

[16] Frank H Netter. *Netter Atlas de Anatomia Humana*. Elsevier, 2011.

[17] Walter F Boron and Emile L Boulpaep. *Medical Physiology, 2e Updated Edition*. Elsevier Health Sciences, 2012.

[18] CC Johnson, FM Fordyce, and AG Stewart. Environmental controls in Iodine Deficiency Disorders - project summary report. 2003.

[19] Bova D Dillehay GL Ward WF, Henkin RE. Basic principles of radiation biology. *Nuclear Medicine*, pages 507–522, 2006.

[20] Richard J Robbins and Martin J Schlumberger. The evolving role of 131I for the treatment of differentiated thyroid carcinoma. *Journal of Nuclear Medicine*, 46(1):28S–37S, 2005.

[21] Markus Luster, SE Clarke, M Dietlein, M Lassmann, P Lind, WJG Oyen, J Tennvall, and E Bombardieri. Guidelines for radioiodine therapy of differentiated thyroid cancer. *European journal of nuclear medicine and molecular imaging*, 35(10):1941–1959, 2008.

[22] Dossier de Patologia Doenças da Tiróide, 2008. http://medicosdeportugal.saude.sapo.pt/content_files/cms/pdf/pdf_1f71e393b3809197ed66df836fe833e5.pdf.

[23] Cancer.Net. Thyroid Cancer, 2013. http://www.cancer.net/cancer-types/thyroid-cancer.

[24] RH Cobin, H Gharib, DA Bergman, OH Clark, DS Cooper, GH Daniels, RA Dickey, DS Duick, JR Garber, ID Hay, et al. AACE/AAES medical/surgical guidelines for clinical practice: management of thyroid carcinoma. American Association of Clinical Endocrinologists. American College of Endocrinology. *Endocrine practice: official journal of the American College of Endocrinology and the American Association of Clinical Endocrinologists*, 7(3):202, 2001.

[25] ML Carcangiu, TH Steeper, G Zampi, and J Rosai. Anaplastic thyroid carcinoma. A study of 70 cases. *American journal of clinical pathology*, 83(2):135–158, 1985.

[26] Fernando Rodrigues, Edward Limbert, Ana Paula Marques, Ana Paula Santos, Carlos Lopes, Elizabete Rodrigues, Francisco Carrilho, Lucilia Salgado, Maria João, et al. Protocolo de tratamento e seguimento dos carcinomas diferenciados da tiróide de origem folicular. *Acta Méd Port*, 18(1):3–18, 2005.

[27] Leslie H Sobin, Mary K Gospodarowicz, and Christian Wittekind. *TNM classification of malignant tumours*. Wiley. com, 2011.

[28] MD Ringel and PW Ladenson. Controversies in the follow-up and management of well-differentiated thyroid cancer. *Endocrine-Related Cancer*, 11(1):97–116, 2004.

[29] Ernest L Mazzaferri and Robert L Young. Papillary thyroid carcinoma: A 10 year follow-up report of the impact of therapy in 576 patients. *The American journal of medicine*, 70(3):511–518, 1981.

[30] Leslie J DeGroot, Edwin L Kaplan, Francis H Straus, and Manan S Shukla. Does the method of management of papillary thyroid carcinoma make a difference in outcome? *World journal of surgery*, 18(1):123–130, 1994.

[31] Cornelius JC Nel, Jon van Heerden, John R Goellner, William M Gharib, Hosseinand McConahey, William F Taylor, and Grant Clive S. Anaplastic carcinoma of the thyroid: a clinicopathologic study of 82 cases. In *Mayo Clinic Proceedings*, volume 60, pages 51–58. Elsevier, 1985.

[32] SM Seidlin, E Oshry, and AA Yalow. Spontaneous and experimentally induced uptake of radioactive iodine in metastases from thyroid carcinoma: a preliminary report. *The Journal of Clinical Endocrinology*, 8(6):423–432, 1948.

[33] R Coliez, M Tubiana, and S Sung. Disappearance of pulmonary metastases of a thyroid cancer under the action of radioactive iodine 131I. *Journal de radiologie, d'électrologie & archives d'électricité médicale*, 32(3-4):396, 1951.

[34] R Coliez, M Tubiana, and J Dutreix. Problems of dosimetry posed by the utilization of radioactive iodine in the treatment of cancer of the thyroid. *Journal de radiologie, d'électrologie & archives d'électricité médicale*, 35(1-2):22, 1954.

[35] R Coliez, M Tubiana, J Dutreix, and J Guelfi. Results of examination of 85 cases of cancer of the thyroid with radioactive iodine. *Journal de radiologie, d'électrologie & archives d'électricité médicale*, 32(11-12):881, 1951.

[36] M Tubiana, R Perez, C Parmentier, and JP Monnier. The survival of patients with thyroid cancers treated with radioactive iodine. apropos of 147 cases followed up for more than 5 years. *La Presse médicale*, 76(42):1999, 1968.

[37] Ian D Hay, Geoffrey B Thompson, Clive S Grant, Eric J Bergstralh, Catherine E Dvorak, Colum A Gorman, Megan S Maurer, Bryan McIver, Brian P Mullan, Ann L Oberg, et al. Papillary thyroid carcinoma managed at the Mayo Clinic during six decades (1940–1999): temporal trends in initial therapy and long-term outcome in 2444 consecutively treated patients. *World journal of surgery*, 26(8):879–885, 2002.

[38] Ernest L Mazzaferri. Thyroid remnant 131I ablation for papillary and follicular thyroid carcinoma. *Thyroid*, 7(2):265–271, 1997.

[39] M Mostafa. Radioactivity calculations for production of 131I by neutron irradiation of tellurium targets. *Radiochemistry*, 51(3):313–320, 2009.

[40] Victor R Preedy, Gerard N Burrow, and Ronald Ross Watson. *Comprehensive handbook of iodine: nutritional, biochemical, pathological and therapeutic aspects*. Access Online via Elsevier, 2009.

[41] Fisher Scientific. Material Safety Data Sheet - Iodine, July 2009. http://dept.harpercollege.edu/chemistry/msds1/Iodine%20Fisher.pdf.

[42] John Harte. *Toxics A to Z: A guide to everyday pollution hazards*. Univ of California Press, 1991.

[43] MM Bé et al. Table of Radionuclides, Bureau International des Poids et Mesures (BIPM), Monographie BIPM-5, Vol. I. Technical report, BNM-LNHB/CEA, 2004, ISBN: 2-7272-0200-8, 2004.

[44] Anna Wyszomirska. Iodine-131 for therapy of thyroid diseases. Physical and biological basis. *Nuclear Medicine Review*, 15(2):120–123, 2012.

[45] Peter F Sharp, Howard G Gemmell, and Alison D Murray. Practical Nuclear Medicine, ed. 3. 2006.

[46] Perkin Elmer. Iodine-131 Handling Precautions. http://shop.perkinelmer.com/content/pdfs/english/iodine131.pdf.

[47] NW Johns, JH Gregson, GC Foster, CH Jaimet, and HG Thode. Radioiodine and Thyroid. *Canadian Medical Association Journal*, 68(2):132, 1953.

[48] Laélia Campos and Frank da Silva. Dosimetry in thyroid follicles due to low-energy electrons of iodine using the Monte Carlo method. *Radiologia Brasileira*, 41(6):403–407, 2008.

[49] Perry Sprawls. *The Physics and Instrumentation of Nuclear Medicine*. University Park Press, 1981.

[50] David S Cooper, Gerard M Doherty, Bryan R Haugen, Richard T Kloos, Stephanie L Lee, Susan J Mandel, Ernest L Mazzaferri, Bryan McIver, Steven I Sherman, and R Michael Tuttle. Management guidelines for patients with thyroid nodules and differentiated thyroid cancer: The American Thyroid Association Guidelines Taskforce. *Thyroid*, 16(2):109–142, 2006.

[51] Furio Pacini and Maria Grazia Castagna. Diagnostic and therapeutic use of recombinant human TSH (rhTSH) in differentiated thyroid cancer. *Best Practice & Research Clinical Endocrinology & Metabolism*, 22(6):1009–1021, 2008.

[52] The American Thyroid Association Taskforce on Radioiodine Safety; James C Sisson, John Freitas, Iain Ross McDougall, Lawrence T Dauer, James R Hurley, James D Brierley, Charlotte H Edinboro, David Rosenthal, Michael J Thomas, Jason A Wexler, et al. Radiation safety in the treatment of patients with thyroid diseases by radioiodine 131I: practice recommendations of the American Thyroid Association. *Thyroid*, 21(4):335–346, 2011.

[53] Wynn A Volkert and Timothy J Hoffman. Therapeutic radiopharmaceuticals. *Chemical reviews*, 99(9):2269–2292, 1999.

[54] Susan J Mandel, P Reed Larsen, Ellen W Seely, and Gregory A Brent. Increased need for thyroxine during pregnancy in women with primary hypothyroidism. *New England Journal of Medicine*, 323(2):91–96, 1990.

[55] J Kenneth Shultis and Richard E Faw. Radiation shielding and radiological protection. In *Handbook of nuclear engineering*, pages 1313–1448. Springer, 2010.

[56] Jr. George E. Chabot. Shielding of Gamma Radiation, August 2007. http://hps.org/documents/shielding_of_gamma_radiation.pdf.

[57] European Commission. Radiation Protection 97: Radiation Protection Following Iodine-131 Therapy (Exposure Due to Out-Patients or Discharged In Patients), 1998.

[58] R Ravichandran, JP Binukumar, and Amal Al Saadi. Estimation of effective half life of clearance of radioactive Iodine (131I) in patients treated for hyperthyroidism and carcinoma thyroid. *Indian journal of nuclear medicine: IJNM: the official journal of the Society of Nuclear Medicine, India*, 25(2):49, 2010.

[59] HR Maxon 3rd, Emanuela E Englaro, Stephen R Thomas, Vicki S Hertzberg, Jerry D Hinnefeld, LS Chen, H Smith, Dwight Cummings, and Michael D Aden. Radioiodine-131 therapy for well-differentiated thyroid cancer–a quantitative radiation dosimetric approach: outcome and validation in 85 patients. *Journal of nuclear medicine: official publication, Society of Nuclear Medicine*, 33(6):1132, 1992.

[60] MJ Groth. Empirical shielding design data for facilities administering 131I for thyroid carcinoma. *Australasian physical & engineering sciences in medicine/supported by the Australasian College of Physical Scientists in Medicine and the Australasian Association of Physical Sciences in Medicine*, 21(4):170, 1998.

[61] DECRETO-LEI nº180/2002 "D.R. Série-A" 182 (2002-08-08) 5707-5745.

[62] DECRETO-LEI nº165/2002 "D.R. Série-A" 163 (2002-07-17) 5364-5370.

[63] DECRETO-LEI nº222/2008 "D.R. 1ª série" 223 (2008-11-17) 8000-8008.

[64] European Nuclear Society. Half-value thickness (HVL) Definition. http://www.euronuclear.org/info/encyclopedia/h/half-value-thickness.htm.

[65] John H Hubbell and Stephen M Seltzer. Tables of X-ray Mass Attenuation Coefficients and Mass Energy-absorption Coefficients from 1 keV to 20 MeV for Elements Z = 1 to 92 and 48 Additional Substances of Dosimetric Interest. *National Institute of Standards and Technology*, 1996.

[66] MJ Groth. Empirical dose rate and attenuation data for radionuclides in nuclear medicine. *Australasian physical & engineering sciences in medicine/supported by the Australasian College of Physical Scientists in Medicine and the Australasian Association of Physical Sciences in Medicine*, 19(3):160, 1996.

[67] David S Smith and Michael G Stabin. Exposure rate constants and lead shielding values for over 1,100 radionuclides. *Health physics*, 102(3):271–291, 2012.

[68] Michael G Stabin. *Radiation protection and dosimetry: an introduction to health physics*. Springer, 2007.

[69] Charles L Dunford and Robert R Kinsey. NuDat system for access to nuclear data. Technical report, Brookhaven National Lab., National Nuclear Data Center, Upton, NY (United States), 2011.

[70] E Browne and JK Tuli. Nuclear data sheets for A= 99. *Nuclear Data Sheets*, 112(2):275–446, 2011.

[71] JD Huo, XL Huang, and JK Tuli. Nuclear data sheets for A= 67. *Nuclear Data Sheets*, 106(2):159–+, 2005.

[72] Yu Khazov, I Mitropolsky, and A Rodionov. Nuclear data sheets for A= 131. *Nuclear Data Sheets*, 107(11):2715–2930, 2006.

[73] Laurie M Unger and DK Trubey. Specific gamma-ray dose constants for nuclides important to dosimetry and radiological assessment. Technical report, Oak Ridge National Lab., TN (USA), 1982.

[74] M Tschurlovits, A Leitner, and G Daverda. Dose rate constants for new dose quantities. *Radiation protection dosimetry*, 42(2):77–82, 1992.

[75] MM Ninkovic, JJ Raicevic, and F Adrovic. Air kerma rate constants for gamma emitters used most often in practice. *Radiation protection dosimetry*, 115(1-4):247–250, 2005.

[76] ATOMTEX. AT1121, AT1123 Dosimeter. http://www.atomtex.com/sites/default/files/at11211123.pdf.